1

Principles of Molecular Chirality

Jean-Claude Chambron and F. Richard Keene

1.1 General Introduction

Chirality is probably one of the most significant topics in chemistry. The strong connection between chirality and symmetry has made it appealing from the mathematical and aesthetic viewpoints, and the recent interest in topologically chiral interlocked and knotted molecules has increased its intellectual attraction, raising the concept of a hierarchy in chirality [1]. The most fascinating aspect of chirality stems from the dynamic properties of molecules and supramolecular assemblies, rather than their static properties, because they are the cause of many intriguing and sometimes paradoxical issues. At the same time, dynamic chirality is also the most useful topic because of the numerous applications it underpins, from chiral recognition to molecular motors.

Historically, chirality is rooted into crystallography (the concept of hemiedry), and the first breakthrough into the field of molecular chirality was Louis Pasteur's hypothesis that the dissymmetry of a crystal was a consequence of dissymmetry at the molecular level [2]. The second milestone was the Le Bel and van't Hoff model of the tetrahedral carbon atom, which accounted for the chirality of the organic compounds known at that time, and several years later Werner was the first to study and provide evidence for the chirality of metal complexes. The discovery of organic molecules that did not owe their chirality to tetrahedral carbon atoms carrying four different substituents (e.g., allenes, biphenyls, cyclophanes), and of helical structures in nucleic acids and proteins, finally led Cahn, Ingold, and Prelog to establish a general system for the description of chiral structures. Since then, many novel chiral molecules have been reported, and most of them could be described in the frame of the CIP rules. The most notable developments in chirality in recent decades concern aspects of the generation and control of chirality: transfer by supramolecular

Chirality in Supramolecular Assemblies: Causes and Consequences, First Edition. Edited by F. Richard Keene.

interactions; chirality of molecular assemblies (chirality at the supramolecular level or "supramolecular chirality"); and finally, the concept of "topological chirality" brought forward by the development of interlocked and knotted molecules.

This chapter constitutes an introduction to molecular chirality from the rigid geometrical model to the topological model, but also from the isolated molecule to assemblies of molecules. As the first chapter in this book on the causes and consequences of chirality in supramolecular assemblies, it will, nevertheless, not cover all the aspects of chirality transfer – in particular those resulting from a covalent bond formation.

1.2 Geometrical Chirality

A chiral object is the one that does not coincide with its mirror image. The source object and its mirror image are called enantiomorphs. From the point of view of symmetry, enantiomorphic objects can have only rotation axes C_n, $n \geq 1$, as symmetry elements: they are either asymmetric (C_1) or dissymmetric (C_n, $n \neq 1$). There are many natural examples of enantiomorphic objects, the prototypical one being the human hand, the Greek word for which (χειρ) has been used to create the English word "chiral." Molecules are objects at the nanometer scale that are made of atoms connected by chemical bonds. If molecules are considered as rigid nanoscale objects, the definition given above can be very easily transposed to the molecular level, with the term "enantiomorph" being replaced by "enantiomer." However, molecules differ from macroscopic objects according to two criteria: (i) they are not rigid and can encompass a great variety of shapes called conformations, the distribution of which depends on time, temperature, and solvent; (ii) they are not usually handled as a single object, but as populations of very large number of individuals (~ Avogadro number). These two unique characteristics make the definition of molecular chirality not as simple as that of a rigid object (such as a quartz crystal), and therefore it needs further developments in order to be refined [2].

The object molecule can be described at different levels of complexity, which are represented by models [3, 4]. The chemical formula, which uses atomic symbols for the atoms and lines for the bonds (traditionally, dashed lines for the weakest bonds), is no more than what has been termed a molecular graph, a concept derived from mathematics that has been introduced and used fruitfully in various areas of chemistry, in particular in molecular topology (see section 1.3). The structural formula is more informative because it shows the spatial relationships between the atoms and the bonds, which can be, for example, probed by nOe effects in NMR spectroscopy. The most accomplished description of the molecule as a rigid object is the 3D representation resulting from an X-ray crystal structure analysis, as it gives the distances between the atoms (bond lengths), and the angles between bonds. This points to the fact that the image of the molecule we have depends on the observation technique – in particular its timescale, observation conditions such as temperature, but also the state of the observed molecule (solid, solution, gas) [5]. In fact, a large number of molecules, including chiral ones, can be described using the approximation of rigidity (i.e., a rigid model) because fluctuations of atom positions are averaged around a thermodynamic equilibrium value at the observation timescale. In that approximation, as pointed out by Mislow [4], the chirality of the molecule is the chirality of the model, which depends only on the atomic positions, so that in principle the bonds can be ignored. However, the

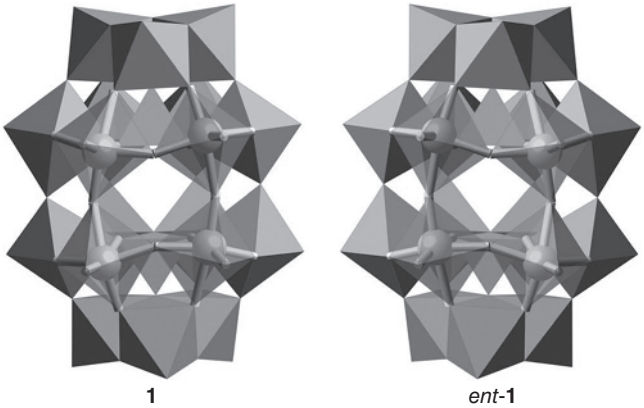

Figure 1.1 *The enantiomers of the chiral Keggin polyoxometallate α-$[P_2Mo_{18}O_{62}]^{6-}$* ***1****. The chirality of this molecule has a dynamic character, which allows the dynamic thermodynamic resolution of a given enantiomer of this hexaanion by interaction with enantiomerically pure cations*

presence of a bond between two atoms indicates that these atoms are closer to each other than if they were not bonded, so that, in practice the bond formalism is very useful for assessing, in a straightforward manner, the chirality of a rigid molecular model. This is the case where, for example, within two identical sets of atoms symmetry-related bonds have different lengths, leading to a distortion of the entire structure. Such an example of chirality due to alternating bond lengths is illustrated by the Keggin polyoxometallate α-$[P_2Mo_{18}O_{62}]^{6-}$ **1** of Figure 1.1 [6].

1.2.1 Origins and Description of Chirality within the Rigid Model Approximation

1.2.1.1 General Considerations

This section will deal with general considerations relating to the description and origins of chirality. Examples selected for their unique chirality properties will be then discussed in more detail in the following sections. Rigidly chiral molecules can only undergo rotations about bonds. They belong to one of the following point groups: (C_1, asymmetric), C_n, D_n, T, O, and I – the latter three being quite rare (see section 1.2.1.3) – which contain only proper symmetry axes as symmetry operations (Table 1.1). Molecular chirality concerns molecules or molecular assemblies featuring a 3D structure. The latter is determined by the interplay between molecular constitution, atom bonding geometry, and intramolecular and intermolecular interactions – including repulsions resulting from strain and steric hindrance. These factors then translate into arrangements of atoms that are either asymmetric (no symmetry element is present) or dissymmetric (with $C_{n>1}$ symmetry elements only) in the 3D space – the necessary but not sufficient (see below) criteria for chirality [2].

The conversion of a planar object into a 3D object can be achieved by either of two possible pathways. It is illustrated in Figure 1.2, starting from a rectangle as an example of a 2D object. Of course the rectangle, lying horizontally, is achiral (D_{2h} symmetry). In the first pathway let us take one of the points of the rectangle, for example its center, and pull

Table 1.1 *Symmetry elements of chiral point groups, the corresponding geometries they are generated from, and maximal symmetries*

Point group (achiral geometrical figure)	Symmetry elements	Symmetry properties
C_1 (general polyhedron)	None	Asymmetric
C_n, n≠1 (cone)	C_n	Dissymmetric
D_n, n≠1 (cylinder)	C_n, n × C_2	Dissymmetric
T (tetrahedron)	4 × C_3, 3 × C_2	Dissymmetric
O (octahedron and cube)	3 × C_4, 4 × C_3, 8 × C_2	Dissymmetric
I (icosahedron and dodecahedron)	6 × C_5, 10 × C_3, 15 × C_2	Dissymmetric

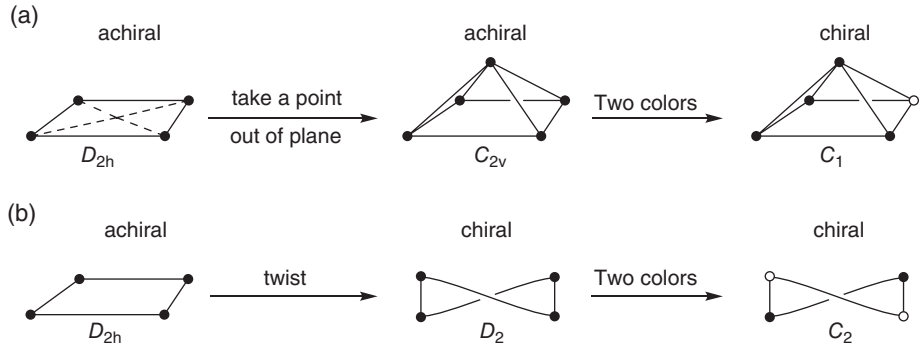

Figure 1.2 *Two pathways for the conversion of a planar object into a 3D object, exemplified by a rectangle. (a) Taking a point out of the plane of the rectangle generates an achiral C_{2v}-symmetric pyramid, of which the desymmetrization to a C_1-chiral object requires the use of two colored vertices (black and white). (b) Twisting converts the rectangle into a D_2-symmetric chiral object, the symmetry of which can be decreased to C_2 by coloring (black and white disks) of selected vertices*

it out of the plane along the vertical direction. This will generate a C_{2v}-symmetric pyramid. This achiral pyramid can be made chiral by changing its constitution – e.g. by coloring selected vertices: a minimum of two colors is required, as shown in Figure 1.2a, which produces an asymmetric (C_1) pyramid. The second pathway arises from a twist to the rectangle along its principal C_2 axis, which makes it a propeller with D_2 symmetry (Figure 1.2b). Hence, unlike the former case, the generation of chirality is simultaneous with the generation of a 3D object. Next, the symmetry is decreased to C_2 by color-differentiation of any two vertices out of the four. Of course, making three vertices of the same color would further decrease the symmetry of the propeller to C_1.

Stacks of an achiral planar object (such as an isosceles triangle, as shown in Figure 1.3) can produce an achiral D_{3h} symmetrical column (b), which upon a regular twist of the individual components is converted into a chiral wreathed column, either left- (a) or right- (c) handed.

In chemical vocabulary, the deformation applied to the rectangle of Figure 1.2a corresponds to a constitutional change as the rectangle (four vertices) has been changed to a

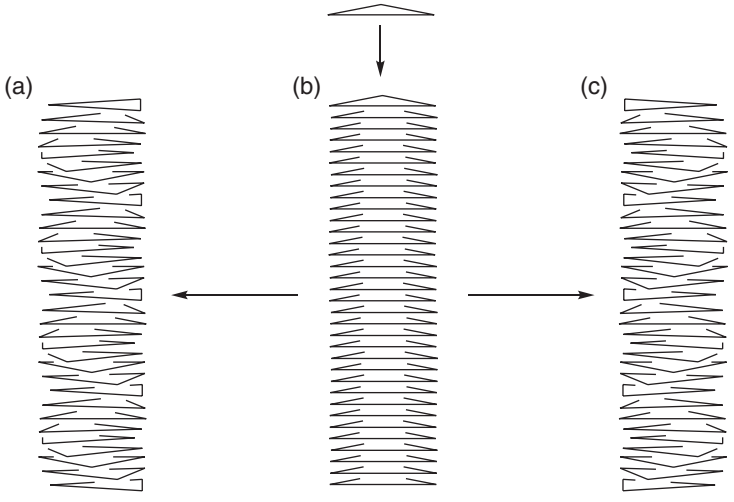

Figure 1.3 *Generating chirality by making (b) stacks of a planar triangular figure, followed by twisting of the resulting column either anticlockwise (a) or clockwise (c)*

pyramid (five vertices), whereas in the case of Figure 1.2b it corresponds to a conformational change as the twisted object has the same number of vertices and faces. Twisting may result from various mechanisms, such as rotations about bonds or variations in bond lengths – and in the case of molecular assemblies, from the generation of a curvature because of intermolecular attractions or repulsions.

The two basic processes of Figure 1.2 can be illustrated in the construction of the mirror-image molecular parallelepipeds $[Zn_2\text{-}\mathbf{2}]_4$ shown in Figure 1.4 by self-assembly of Zn(porphyrin) covalent dimers (*R*)-Zn_2-**2** and (*S*)-Zn_2-**2** driven by the Zn-pyridyl interaction [7]. The vertices of the cubes are occupied by Zn porphyrin (ZnPor) subunits, whereas four parallel edges are formed either by *meso* C–C single bonds or the *meso* C–(4-pyridyl)–ZnPor bond sequence. The bis(porphyrin) subunits are twisted by 90° with respect to each other, while each Zn^{2+} cation has a pyramidal N5 environment in the assembly.

The specification of chirality was formalized by Cahn, Ingold, and Prelog using (in the first instance) the "chirality model," which involves three stereogenic elements of chirality: the center, the axis, and the plane [8]. The chirality model of molecules is based on the tetrahedron, which is also the minimal 3D polyhedron [9]. In the first case (asymmetry, Figure 1.5) the perfect tetrahedron of T_d symmetry needs four different achiral vertices (A, B, C, and D) to be C_1 chiral (asymmetric constitution). Another possibility is to consider a tetrahedron of C_1 symmetry, in which all six edges have different lengths (asymmetric arrangement of the atoms). In practice, the asymmetric tetrahedron results both from asymmetric constitution and atom arrangement (Figure 1.5d).

In the second case (dissymmetry, Figure 1.6), elongation along one of the C_2 symmetry axes of the tetrahedron of Figure 1.5a decreases its symmetry to D_{2d}, and therefore only two different achiral substituents (A and B) are now needed to make it C_2-symmetric chiral. In addition, the D_{2d} elongated tetrahedron can also be made chiral without the need of substituents, by differentiating another pair of edges that are related by the main C_2 axis (z direction). This is done by compressing the tetrahedron of Figure 1.6a in the y direction,

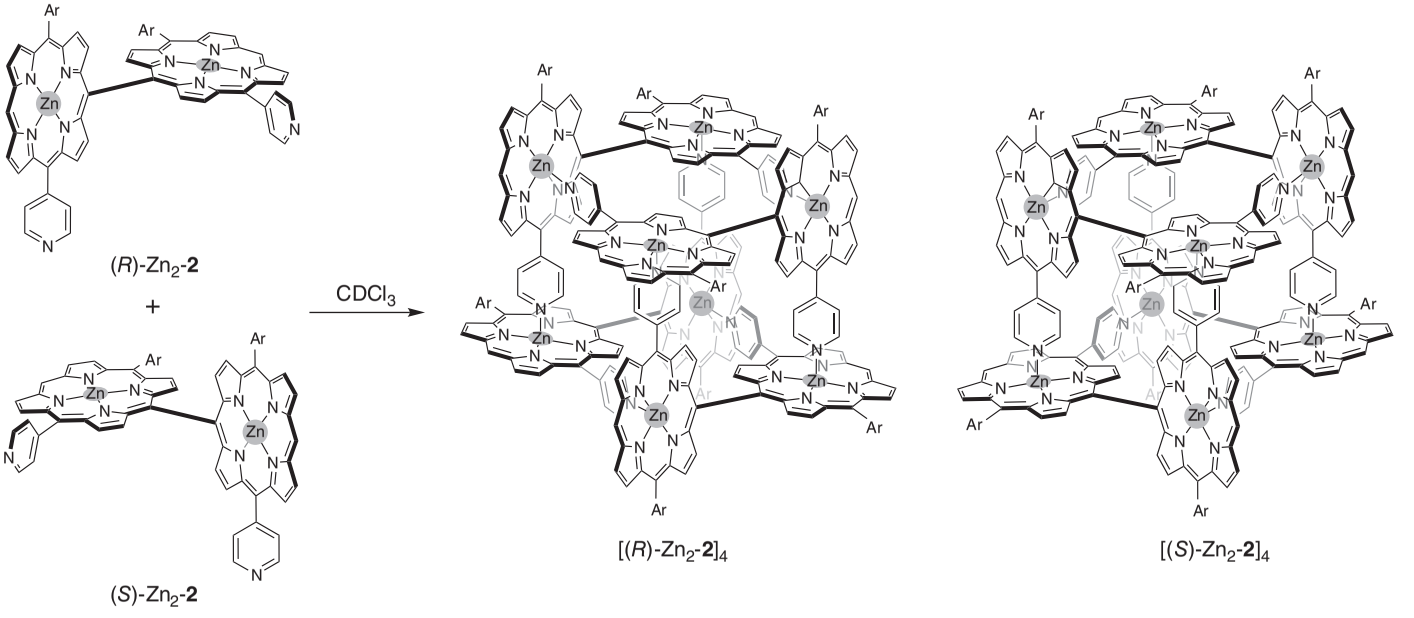

Figure 1.4 *Formation of homochiral assemblies [(R)-Zn_2-**2**]$_4$ and [(S)-Zn_2-**2**]$_4$ from twisted Zn(porphyrin) covalent dimers (R)-Zn_2-**2** and (S)-Zn_2-**2**, based on the Zn^{2+}-pyridyl interaction*

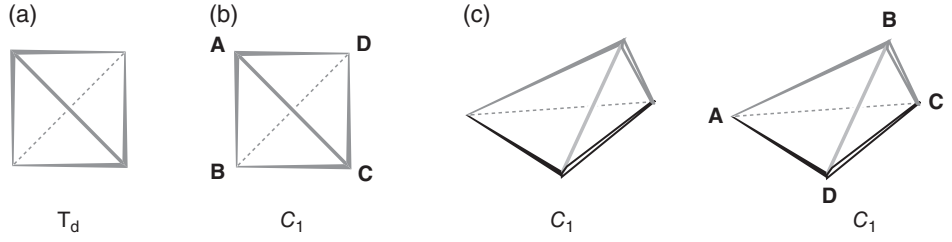

Figure 1.5 *Making the regular, T_d symmetric, tetrahedron (a) asymmetric: (b) by assigning the vertices four different labels; (c) by differentiating the lengths of all six edges using six different "colors"*

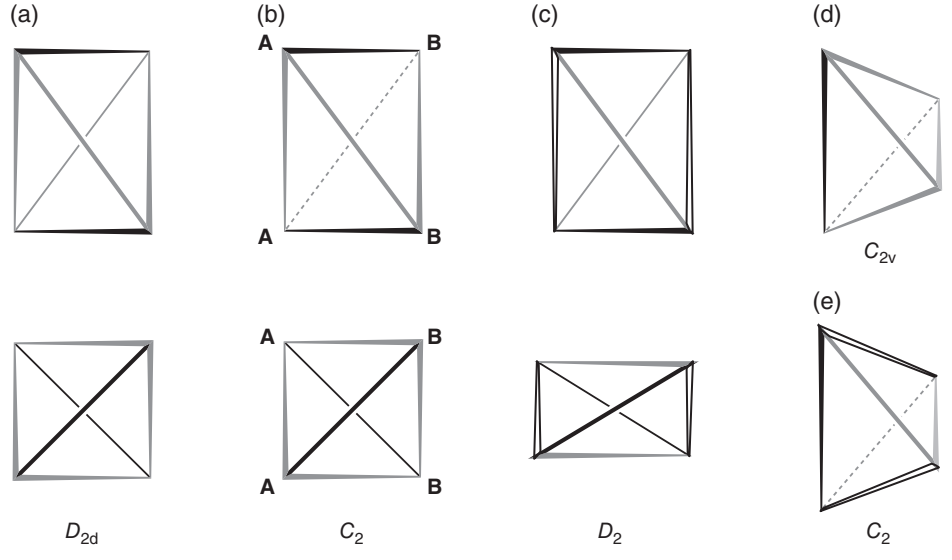

Figure 1.6 *Desymmetrization of the regular tetrahedron. (a) Elongation along one of the C_2 symmetry axes makes the two edges that are perpendicular to it (colored in black) different from the others. A view from the top is shown below the side view. (b) This D_{2d}-symmetric tetrahedron is made C_2-symmetric by labeling the four edges with two different labels, A and B. (c) It can be made D_2-symmetric by further coloring (in white) two edges that are symmetry related by the main C_2 axis. As shown in the top view below, this corresponds to a second elongation, along the C_2' axis. (d) The symmetry of tetrahedron (a) is further decreased to C_{2v} by differentiating a third edge (colored in light gray). (e) The latter is made C_2-chiral by coloring in white two edges that are related by the C_2 symmetry axis, leaving the two others in dark gray*

which removes its symmetry planes. The resulting tetrahedron (Figure 1.6c) is D_2-symmetric. Decreasing the symmetry of the D_{2d} tetrahedron further by moving symmetrically two vertices closer to each other as shown in Figure 1.6d, produces a C_{2v}-symmetric tetrahedron, which is made C_2-symmetric chiral by differentiating a pair of C_2 symmetry-related edges (Figure 1.6e).

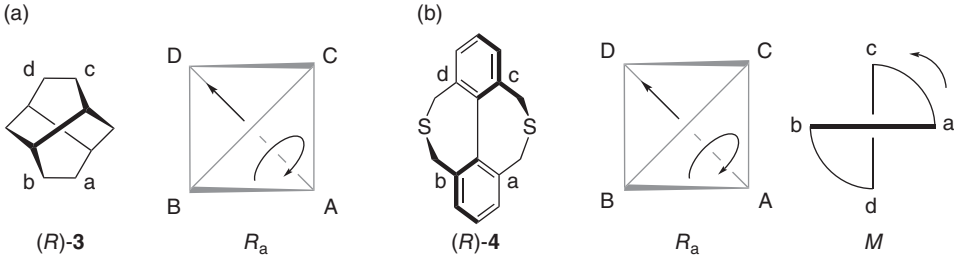

(*R*)-**3** R_a (*R*)-**4** R_a *M*

Figure 1.7 *Description of chirality using the chirality axis as stereogenic unit (a, b), and comparison with the description of chirality by identification of a twist (b). a) (+)-Twistane* ***3****. The chirality axis bisects [a, b] and [c, d]. b) A* D_2*-symmetric doubly bridged biphenyl* ***4****. The chirality axis is the biphenyl Ar-Ar bond. In both cases the positions of a and b are arbitrary, however the CIP rules govern those of c and d. Biphenyl (b) is also a molecular propeller, the conformation of which is* M

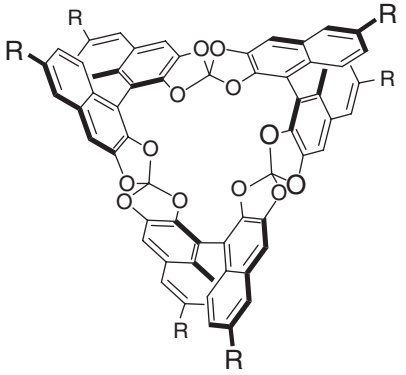

(*R*,*R*,*R*,*R*,*R*,*R*)-**5** (R = H or *n*Bu)

Figure 1.8 *The 3D triangular Janus cyclophane* ***5*** *is made by connecting three homochiral binaphthol-derived subunits by three carbon bridges. The configuration of all six chirality axes is* R

Figure 1.7 illustrates how two molecules, the 3D structures of which arise from different factors, are described using the same formalism (the chirality model) – in this particular case, the chiral axis. (+)-Twistane **3** (Figure 1.7a) owes its chirality to a highly symmetrical arrangement of sp^3 carbon atoms in space. The ansa-biphenyl **4** of Figure 1.7b is D_2-symmetric chiral due to strain-relieving twisting. Both molecules have the same configuration (R_a), which is obtained from the chirality model. In addition, the biphenyl can also be considered as a molecular propeller, and as its 3D structure is of conformational origin, it is best described using the *M*/*P* nomenclature. From the CIP rules, it is the *M* conformation that corresponds to the R_a configuration.

An additional illustration of the chirality axis is given in Figure 1.8, which shows a tris(spiroorthocarbonate) cyclophane (**5**) made in low yield by condensation of (*R*)-2,2′,3,3′-tetrahydroxy-1,1′-binaphthyl with dichlorodiphenoxymethane as the carbon source in refluxing toluene [10]. The resulting D_3-symmetric cyclophane has six chirality axes, three

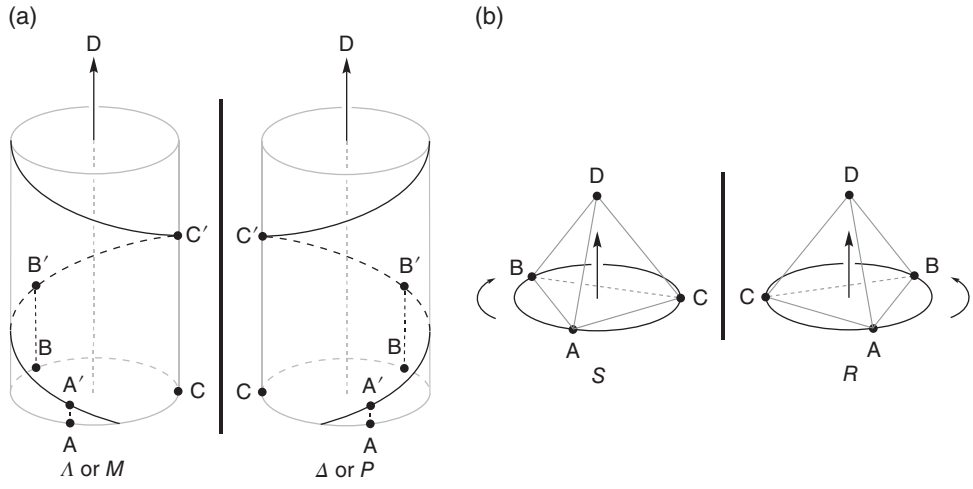

Figure 1.9 *Two different ways to define and orient the 3D space and the analogies between them. (a) Definition and orientation of the 3D space within the helicity model: generation of a helix and description of helical chirality using the Λ, Δ or* M, P *descriptors. (b) Chirality model: reduction of the stereogenic unit to a tetrahedron substituted with four different substituents (descriptors* S *and* R*). The vertical arrows are oriented towards the face from which the ABC plane must be seen. In (a) the D point has been sent to the infinite. Note that, when both models can be equally applied, there is no relationship between the helicity and chirality descriptors, except in the case of the biaryls, where* M *and* P *correspond respectively to* R *and* S

of conformational origin from the binaphthyl components, and three of configurational origin from the spiroorthocarbonate connections, which are interdependent. This molecule features two back-to-back aromatic concavities, which were shown by X-ray crystallography to be able to complex two C_{60} guests via multivalent π-π interactions.

The other model that was devised by Cahn, Ingold, and Prelog is the "helicity model," which proved subsequently to be extremely relevant in describing the chirality of a great variety of molecules and polymers, in spite of the fact that – at the time it was proposed – examples of helical nanoscale objects were rare [8]. From the mathematical viewpoint, a helix results from the combination of a rotation and a translation, and can be cylindrical (C_2 symmetry) or conical (C_1 symmetry). Once a helical structure is clearly identified, for example as a secondary structure, the sense of chirality is given by the helical path. If a clockwise rotation produces a translation away from the observer (following the sequence A′, B′, C′ in Figure 1.9a), the sense of chirality is *P* or *Δ*; if the same effect is produced by a counterclockwise rotation, the sense of chirality is *M* or *Λ*. Note that *P* and *M* descriptors generally apply to conformations and to the so-called secondary structures, and that the *Δ* and *Λ* descriptors are used for the configurations of transition metal complexes.

Natural macromolecular compounds such as DNA, polypeptides, and amylose, as well as synthetic examples such as polyacetylenes and polyisocyanates, can take up helical shapes [11]. This is also the case with molecular compounds like foldamers [12], helicenes [13], and helicates [14] (Figure 1.10). Larger structures encompass at least a full helix turn. By contrast, the smaller members of these families of molecules do not incorporate a 360° turn

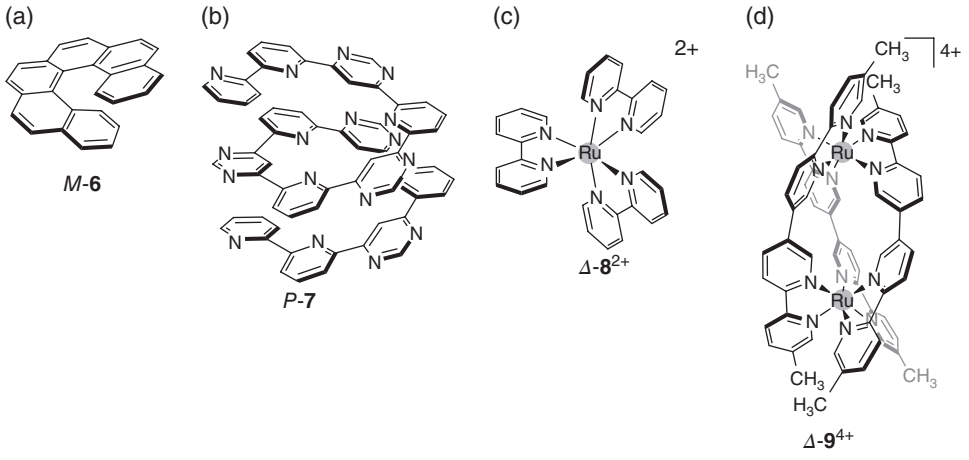

Figure 1.10 *Examples of helically chiral molecules and molecular propellers. (a) [6]Helicene* ***6****. (b) Foldamer* ***7*** *based on alternating pyridine and pyrimidine subunits. (c) The* $[Ru(bipy)_3]^{2+}$ *coordination complex (*$\mathbf{8}^{2+}$*), where bipy is 2,2′-bipyridyl, is a* C_3*-symmetric propeller. (d) Connecting two homochiral* $[Ru(bipy)_3]^{2+}$ *subunits through the positions 4 and 4′, respectively, of the bipy ligands produces a fragment of the triple helical dinuclear complex* $\mathbf{9}^{4+}$ *in which each quaterpyridine ligand has the same helical conformation*

and actually represent helical fragments: This is notably the case of the so-called molecular propellers [15] (Figure 1.10c), or of molecules that feature a simple twist (Figure 1.7b). Helicity can also manifest itself at the supramolecular level, for example in the case of helical stacks of achiral molecules. It is important to note at this stage that the formation of hierarchically organized chiral supramolecular structures can make the connection between nanoscopic and microscopic or macroscopic chirality (e.g., chiral molecular gels or chiral mesophases). The highest symmetry molecular propellers belong to the D_n symmetry point groups. Among D_n-symmetric propellers, those belonging to the D_2 symmetry point group are worth highlighting because they make the connection between the helicity model and the chirality model, as both models apply in that case (see Figure 1.7b).

As is the case for DNA, many helically chiral molecular compounds feature double or triple helices. This is particularly the situation for the helicates in which polychelate ligands take up helical conformations upon bridging at least two metal cations. This is illustrated in Figure 1.10d by the dinuclear Ru^{2+} complex of a quaterpyridine ligand ($\mathbf{9}^{2+}$) [16].

After this short overview of the origins and description of chirality we shall detail several examples that illustrate the two basic principles of formation of chiral structures in the 3D space shown in Figure 1.2 – that is, desymmetrization by constitution and desymmetrization by twisting.

1.2.1.2 Desymmetrization by Constitution

Figure 1.11 shows the grid-type tetranuclear metal-ligand assembly $[Os_2Fe_2(\mathbf{10})_4]^{8+}$ made from a "fused" bis(terpyridine)-like ligand (**10**) (in which two 2,2′-bipyridine moieties are bridged by a central pyrimidinyl fragment), and two different metal ions (Os^{2+} and Fe^{2+}),

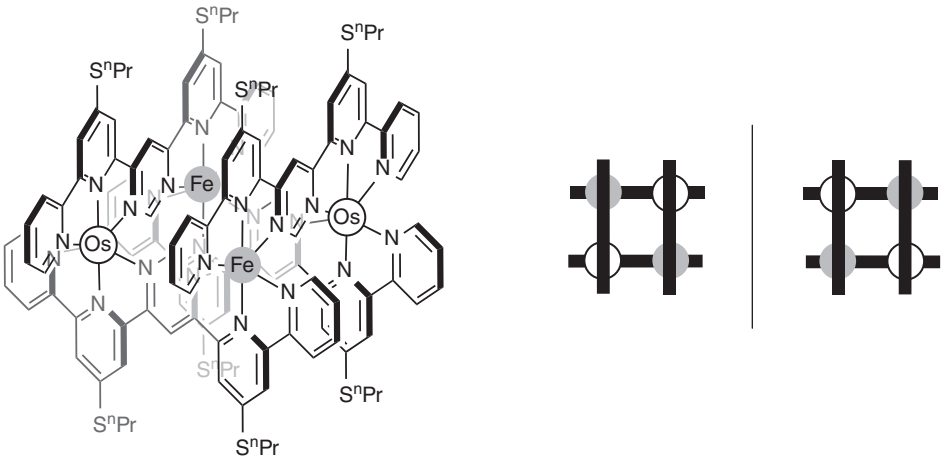

Figure 1.11 *The chirality of the grid-type tetranuclear complex $[Os_2Fe_2(\mathbf{10})_4]^{8+}$ of the "fused" bis(terpyridine)-like ligand* ***10***

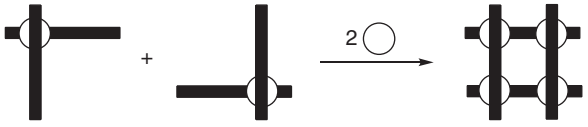

Figure 1.12 *The achiral D_{2h}-symmetric molecular grid is formed from two homochiral halves of mononuclear corner complexes with the bischelate ligands (black elongated rectangles) by addition of two metal cations that are identical to those involved in the starting homochiral complexes*

the pairs of identical metal centers being located on a diagonal [17]. This was done in a straightforward manner by introducing the metal centers in the order of increasing lability – reacting at first the di-chelate with NH_4OsCl_6 in 1 : 1 ratio, thus generating a corner-type chiral mononuclear complex, followed by the addition of $Fe(BF_4)_2$ (2 equivalents). Interestingly, the reaction proceeded stereoselectively to produce the chiral D_2-symmetric tetranuclear complex, as only corner-type precursors of the same handedness react with each other, excluding the formation of achiral *meso* C_{2v} assemblies. It is noteworthy that the tetra-homonuclear assembly represents a stereochemical curiosity, as it can be disconnected into two homochiral mononuclear di-chelate complex subunits. This illustrates the stereochemical paradox called "la coupe du roi" (Figure 1.12) [18].

Another remarkable case of desymmetrization by molecular constitution is offered by the higher order fullerenes. Fullerenes were unprecedented examples of molecules featuring a closed-shell structure. C_{60} itself has icosahedral I_h symmetry and is therefore achiral, but several higher order fullerenes such as $\mathbf{C}_{76}$, have been isolated and characterized. $\mathbf{C}_{76}$, which derives from C_{60} by incorporation of 16 additional C atoms, has D_2 symmetry, as shown by ^{13}C NMR (19 lines of equal intensity), and its chirality arises from its oblong,

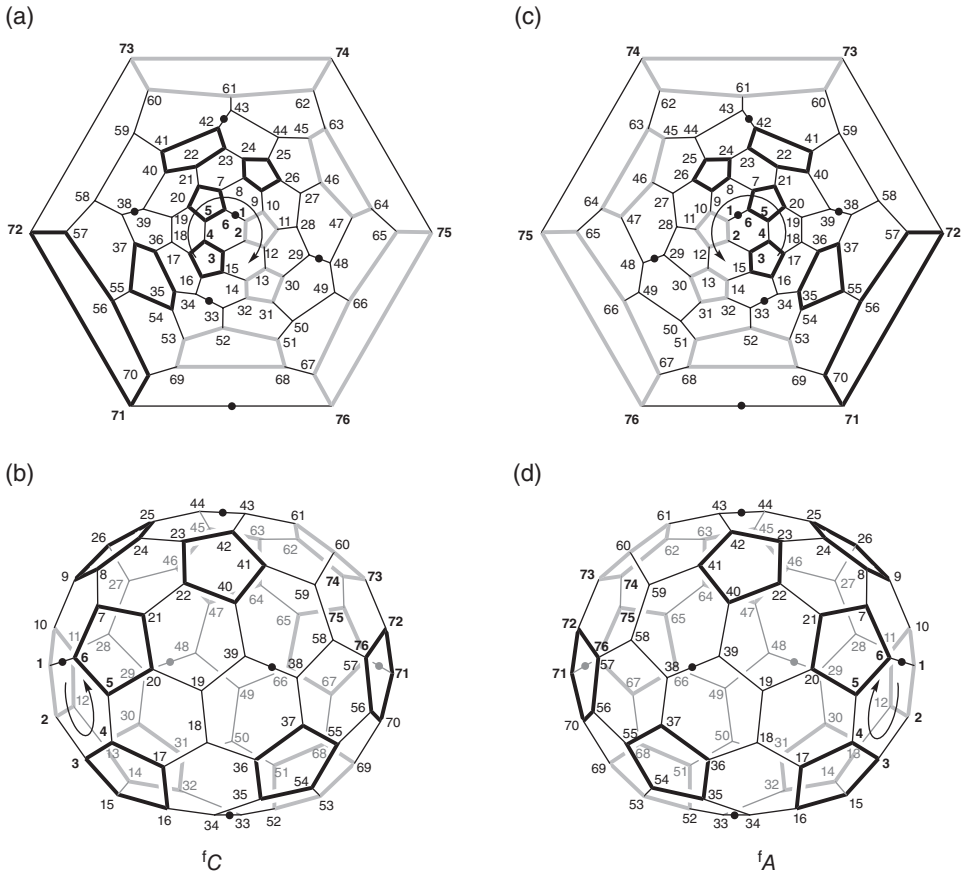

Figure 1.13 *Schlegel diagrams (a and c) and perspective representations (b and d) of the corresponding enantiomers of* $\mathbf{C}_{76}$*. The double bonds have been omitted for clarity. Five-membered rings have been highlighted in bold (black for the front ones, light gray for the rear ones in (b) and (d). The Schlegel diagram is obtained by opening the C71 to C76 six-membered ring and looking down the C1 to C6 analog (bold labels). The descriptor is* ^{f}C *if the C1 to C6 sequence is clockwise and* ^{f}A *if it is the opposite. The intersection of the three* C_2 *axes with the bonds have been materialized by the black dots: the vertical axis crosses C43–C44 and C33–C34, one horizontal axis crosses C1–C6 and C71–C76, and the other crosses C38–C39 and C29–C48*

helically twisted structure (Figures 1.13b to 1.13d) [19]. The enantiomers of $\mathbf{C}_{76}$ were resolved through the HPLC separation of the two diastereomers obtained by regioselective functionalization of $\mathbf{C}_{76}$ with an optically active malonate, followed by an electrochemical retro-Bingel reaction performed on each isolated diastereomer to release each optically pure $\mathbf{C}_{76}$. In principle, as all carbon atoms are pyramidalized, the configuration of the fullerene can be described by listing the absolute configuration (*R* or *S*) of each stereogenic center. The latter is obtained by developing the corresponding hierarchic directed graph which, however, is a cumbersome task.

Therefore a simplified procedure, which uses a single descriptor, has been developed which relies on the fact that the numbering schemes of fullerenes are helically chiral (Figures 1.13a to 1.13c), and can be used to differentiate between enantiomeric fullerenes. Whereas two isometric mirror-symmetric numbering schemes can be applied to an achiral parent fullerene such as C_{60}, a unique one is associable with a specific enantiomer of an inherently chiral carbon spheroid. Depending on whether the path traced from C(1) via C(2) to C(3) of this numbering is clockwise (C) or anticlockwise (A), the descriptors are defined as ^{f}C and ^{f}A. Figures 1.13a and 1.13c show the Schlegel diagrams of the enantiomers of $\mathbf{C}_{76}$ viewed through the opening of the six-membered C71–C72–C73–C74–C75–C76 cycle in the direction of its C1–C2–C3–C4–C5–C6 analog. The sense of the latter sequence (clockwise or anticlockwise) gives the chirality descriptor ^{f}C or ^{f}A. As $\mathbf{C}_{76}$ is D_2-symmetric, it has three C_2 symmetry axes that are orthogonal to each other.

Concave, bowl-shaped molecules represent a very important family of receptors and precursors of receptors that may display chirality [20]. Examples are resorcinarenes, calixarenes, cyclotribenzylenes and cyclotriveratrylenes, tribenzotriquinacenes [21], sumanenes [22], subphthalocyanines [23] and receptors built from these compounds – such as the cryptophanes made by dimerization of functionalized cyclotribenzylenes [24], or molecular capsules assembled by hydrogen bonding between urea-functionalized calix[4]arenes [25]. As concave molecules are nonplanar, they can be made chiral just by rim orientation. The simplest geometrical model of a concave molecule is a tetrahedron with an "empty" ABC face opposed to the D vertex [26]. Calix[4]arenes carrying at least two different substituents in the *para* positions of the phenol rings, or having even a single *meta* substituent, such as **11** (Figure 1.14a) [27], cryptophanes carrying two different substituents at the *meta* positions of the phenylene rings, such as **12** (Figure 1.14b) [24] – just to mention a few – are examples of concave molecules that owe their chirality to rim orientation. These compounds have been qualified as "inherently chiral," because their chirality (which does not depend on the presence of chiral substituents) is a property of the overall structure [26]. However, this expression may be misleading as bowl inversion, when it is possible, reverses the sense of chirality: therefore concave molecules are better described under the heading of conformational chirality [28]. The recommended descriptors to characterize these molecules are *P* and *M* [8]. Rim orientation of achiral concave molecules may also result from the concerted orientation of substituents, for example by a directed network of hydrogen bonding. The self-assembled molecular capsule $(\mathbf{13})_2$ of Figure 1.14c is obtained by Et_4N^+-templated head-to-head dimerization of two urea-substituted calix[4]arene (**13**) components [25].

Cyclodextrins are concave macrocyclic oligomers of *D*-glucose, and are therefore enantiomerically pure compounds. The recent development of efficient methods for the selective functionalization of their primary rim has led, in particular, to the synthesis of α-cyclodextrins carrying three different substituents [29]. Figure 1.15 shows an example in which the original primary alcohol functions have been replaced by -PPh_2, -OBn (Bn is CH_2Ph) and -Me groups that alternate twice, which imparts an orientation to the primary rim. Therefore, the modified cyclodextrin has two diastereomers **14a** and **14b**, because the chirality due to rim orientation is superposed on the chirality of the native cyclodextrin backbone. The resulting molecule can be considered a diphosphine ligand, and indeed it was used in the Tsuji–Trost allylation reaction. It was shown that opposite orientations of the primary rim led to opposite enantioselectivities, albeit rather low (30%), whereas the

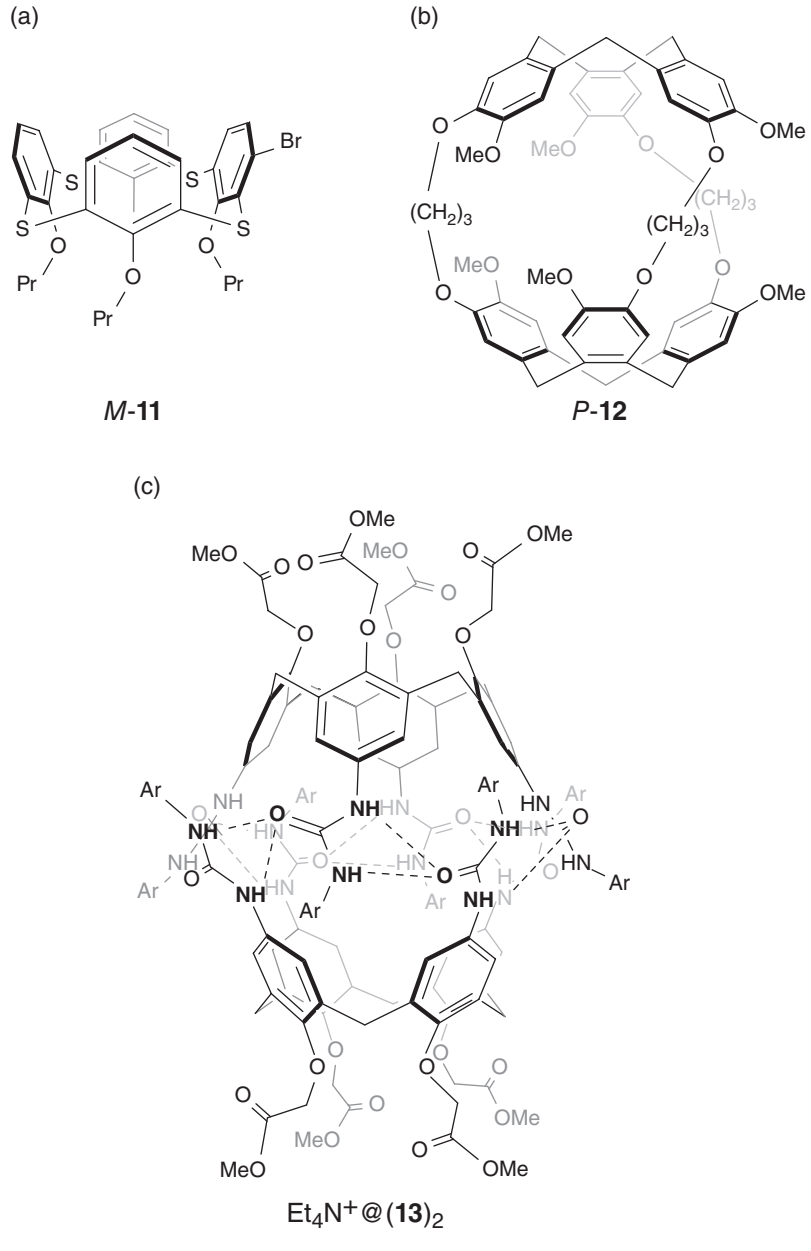

M-**11** *P*-**12**

$Et_4N^+@(\mathbf{13})_2$

Figure 1.14 *Examples of concave chiral molecules. (a) One of the phenyl rings of thiacalix[4]arene* ***11*** *bears a bromine atom in the* meta *position, which destroys the* C_{4v} *symmetry of the parent compound, and makes the corresponding system asymmetric. The propyl groups prevent ring inversion at ambient temperature. (b) Cryptophane-A (****12****) in the chiral,* anti-*configuration* (P). *(c) A head-to-head calix[4]arene dimer (****13****)*$_2$ *via hydrogen bonding between arylurea substituents, that encapsulates* EtN^+ *(removed for clarity; Ar* = p-*tolyl). The methyl acetate substituents maintain the macrocycles in the cone conformation*

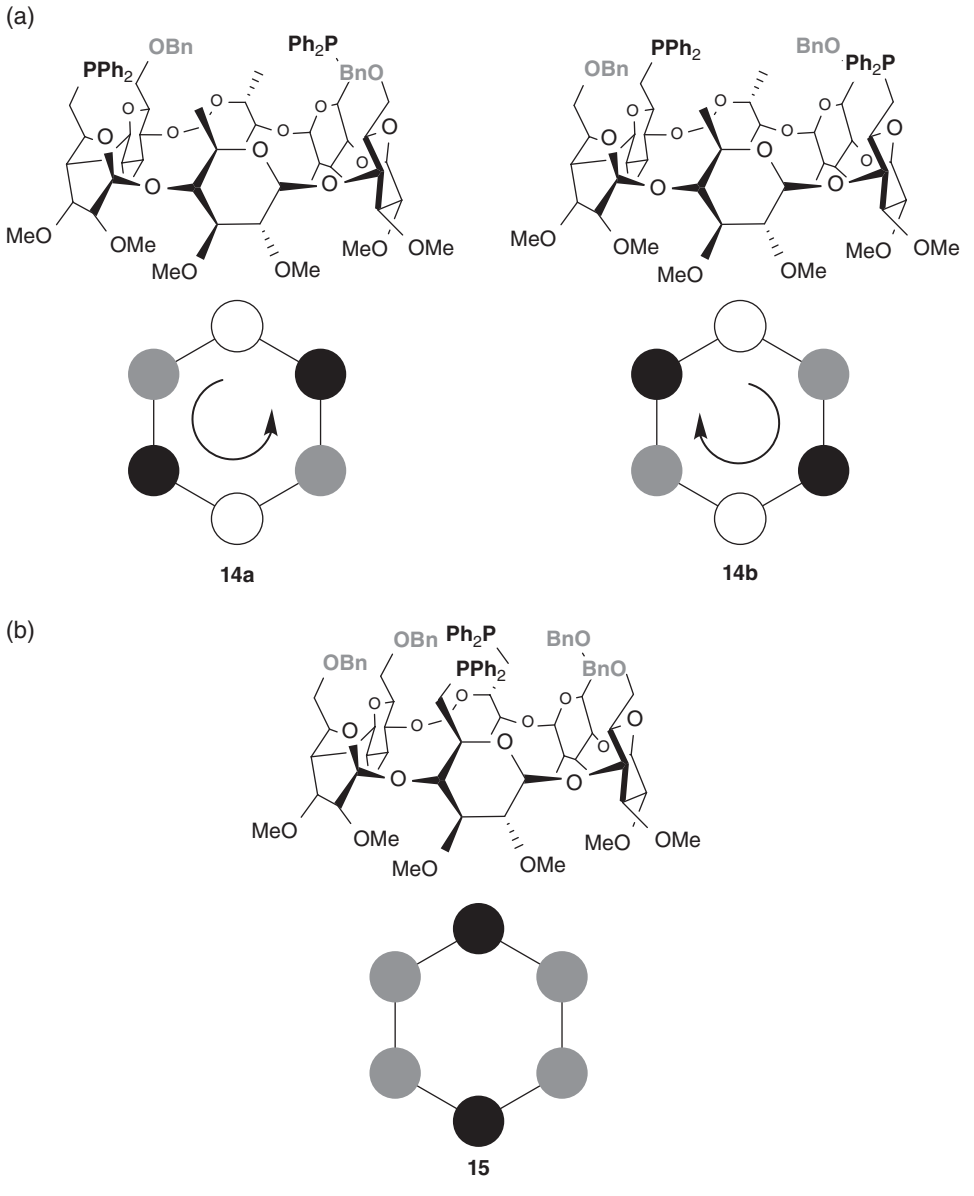

Figure 1.15 *Examples of (a) a pair of diastereomeric α-cyclodextrins (**14a** and **14b**) that differ by the primary rim orientation; (b) Cyclodextrin **15** is chiral; however, the primary rim is not oriented*

corresponding cyclodextrin (**15**) with a σ_h-symmetrical arrangement of two -PPh_2 and four -OBn groups led to no asymmetric induction at all. This pointed to the higher asymmetric character, with respect to the palladium-catalyzed allylation reaction, of the rim orientation by comparison with the cyclodextrin cavity.

1.2.1.3 Desymmetrization by Twisting

Examples of synthetic molecules exhibiting helical chirality are multidecker systems (cyclophanes, etc.) [30], helicates[14] or foldamers [12]. Whereas helicity of multidecker molecules results from constitutional features only, helicity of helicates and foldamers also involve intramolecular interactions as a twisting factor. Helicates are transition metal complexes containing at least two metal centers, and generally feature double- and triple-helical structures, single-helical cases being best described as foldamers. Helical folding of the multichelate strands is directed by the metal centers, the coordination geometry of which orients the ligands in well defined directions of space. Helicates containing at least two metals centers are linear but higher order helicates can show also circular [31] and other geometries, in particular tetrahedral, when they are made of four metal centers that occupy the vertices of a tetrahedron [32]. True helicates are chiral species that incorporate homochiral metal complex subunits. However, they can have diastereomers that differ by the sense of chirality at the metal centers. For example, in the case of dinuclear systems, there are two diastereomers, the enantiomeric pair of helicates (Δ,Δ and Λ,Λ), and the achiral, so-called mesocate (Δ,Λ), containing metal complex subunits that have opposite chirality senses. The formation of a helicate versus a mesocate has been shown to be highly dependent on the nature of the bridge and the connections between the chelates forming a polynucleating ligand strand – in particular *meta*-phenylene bridges strongly favor the helicate. This highlights the role of the ligand bridges in conveying the chiral information between stereolabile metal centers. Figure 1.16 shows two of the three possible diastereomers (excluding enantiomeric pairs) of the tetranuclear Fe^{2+} complex $[Fe_4(\mathbf{16})_6]^{8+}$ with a binucleating diimine ligand (**16**) built *in situ* from the corresponding amine and aldehyde, and bridged by a *p*-terphenylene spacer [33]. All four iron centers have the same chirality in the true helicate, which displays chiral *T* symmetry, whereas the *meso* form, incorporating two Δ and two Λ centers, has achiral S_4 symmetry. In the *T* isomer chelates of the same ligand display the *anti* orientation with respect to each other, and the three phenyl groups of the spacer are arranged with a helical twist that allows for the perfect stereochemical coupling between the metal centers, whereas in the case of the S_4 isomer four of the six bridging ligands have the *syn* orientation.

The diastereomeric ratio of the *T*, S_4, and C_3 diastereomers was ca. 1 : 1 : 1. However, it could be changed by modification of the terphenyl spacers connecting the diimine ligands. The *anti* orientation is favored by introduction of two methyl substituents *ortho* to the central ring, which induce a 60° dihedral angle between adjacent phenyl rings, as a result of a weak van der Waals interaction between the methyl group and the phenyl group of an adjacent ligand [33]. The *syn* orientation is favored by constraining the two phenyl rings attached to the chelate groups to be parallel to each other. This is done by permethylation of the central phenyl ring, which makes it perpendicular to the peripheral rings. Therefore, when dimethylated terphenyl spacers are used, the major diastereomer is the true helicate (*T*-symmetry), whereas when tetramethylated terphenyl spacers are used, the major diastereomer is the *meso* form of S_4 symmetry. Stereochemical coupling between the metal centers is increased in the first case, whereas it is decreased in the second case.

Foldamers are single stranded molecules that can fold in order to take up directed bent conformations. Helicity is the conformational response to avoid steric interactions between overlapping sections of strands. In the case of the helicenes (Figure 1.10a), folding is encoded in the molecular constitution but in true foldamers it is the result of (programmed)

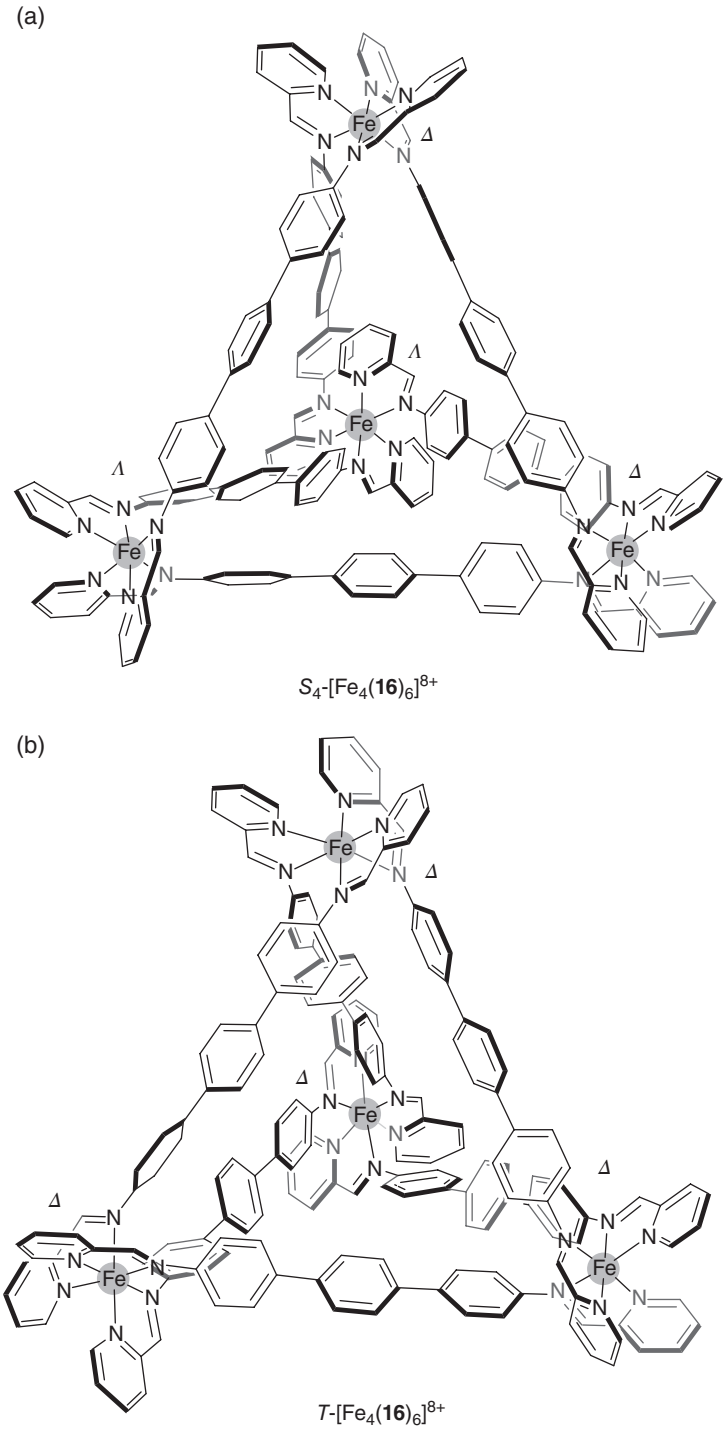

Figure 1.16 *Two diastereomers of the tetranuclear transition metal aggregate* $[Fe_4(\mathbf{16})_6]^{8+}$ *built on four* Fe^{2+} *cations and six binucleating diimine ligands* ***16****. (a) Achiral (Δ, Δ, Λ, Λ)* meso *form, with* S_4 *symmetry. (b) Chiral (Δ, Δ, Δ, Δ) form, with T symmetry*

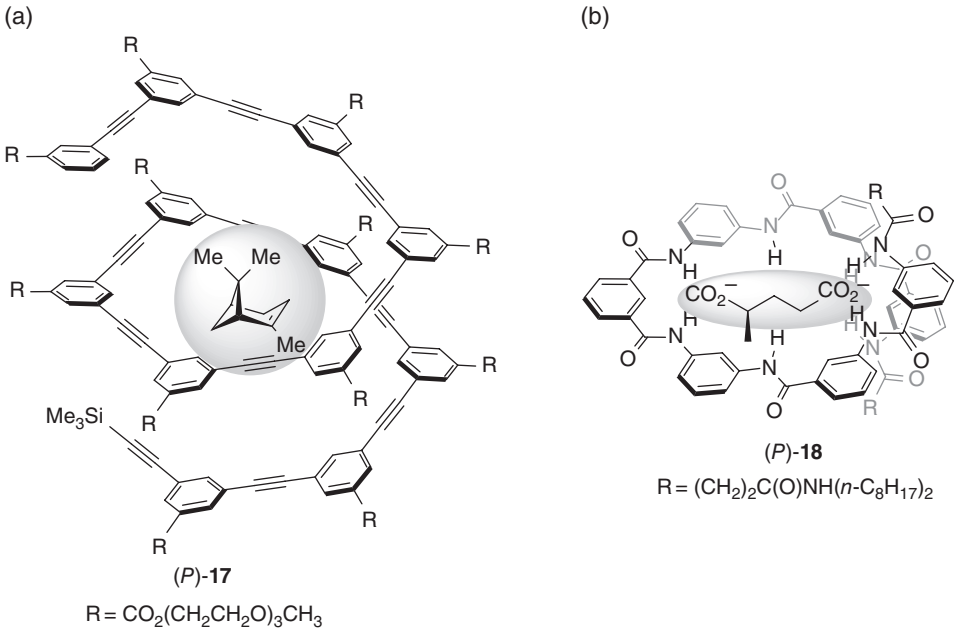

Figure 1.17 *Examples of foldamer hosts, the chirality sense of which is controlled by the chirality sense of the chiral guest. The preferred* P *conformation of the foldamers shown are controlled by (a) (–)-α-pinene in its complex with* ***17****, and (b) D-glutamate in its complex with* ***18***

intramolecular interactions – such as electronic repulsions (Figure 1.10b) or electronic attractions, and hydrogen bonding. When the strand wraps around a molecule, a cation or an anion, folding is the result of intercomponent interactions (such as van der Waals interactions), coordination bonds, and hydrogen bonds. Figure 1.17 shows two representative examples of foldamers that act also as hosts. The arylethynyl system **17** of Figure 1.17a folds around the neutral optically active (–)-α-pinene template [34] as a result of van der Waals and hydrophobic interactions, whereas the oligoarylamide system **18** of Figure 1.17b folds around the optically active D-glutamate dicarboxylate [35] as the result of hydrogen bonding interactions between the amide protons and the anionic carboxylate functions. Foldamers are in general dynamic systems. In the present cases the helicity sense of the foldamers is controlled by the absolute configuration of the optically active guest.

1.2.2 Dynamic and Supramolecular Chirality

1.2.2.1 Enantiomerization Pathways

There are molecules that can encompass enantiomeric conformations under the conditions of observation, and it is this very point that makes molecules unique nanoscale objects. Two cases can be distinguished, depending on the sequence of intermediates that are involved in the interconversion pathway, as they can involve achiral or only chiral species. The first case is classically illustrated by *cis*-1,2-difluorocyclohexane (**19**), the stable chair conformations of which have C_1 symmetry with one fluorine atom in equatorial position

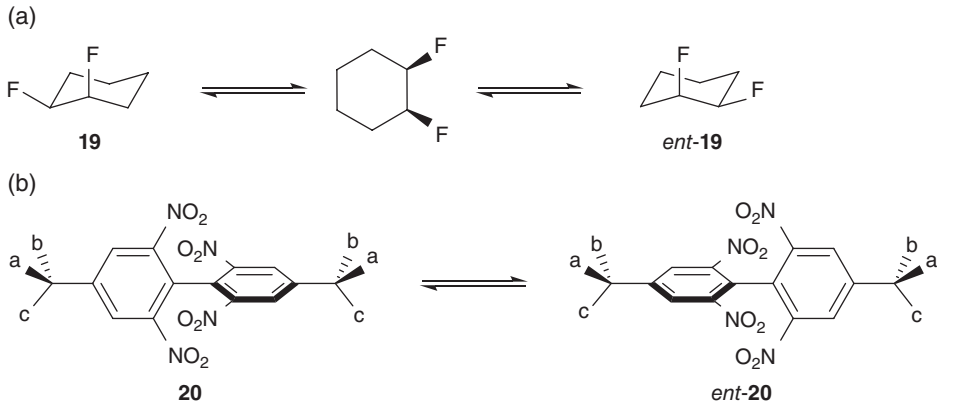

Figure 1.18 *(a) Interconversion of the asymmetric chiral conformations of* cis-*1,2-difluorocyclohexane* ***19*** *to their mirror-image involves an achiral intermediate of C_s symmetry. (b) The generic biphenyl* ***20*** *is chiral-asymmetric in all of its conformations. As a result, interconversion of mirror-image conformations takes place through a chiral pathway. Note that Cabc stands for the menthyl group*

and the other in axial position. Interconversion involves a higher energy achiral intermediate with C_s symmetry (Figure 1.18a). Other examples are provided by the mechanisms of racemization of octahedral transition metal complexes with bidentate ligands – i.e. the Bailar and the Ray–Dutt twists, which involve achiral trigonal prismatic species of D_{3d} and C_{2v} symmetry as intermediates, respectively. The second case is illustrated by the biphenyls of generic formula shown in Figure 1.18b (**20**) [36]. These molecules, composed of three rigid blocks (A, B, and A*; A* being mirror-image of A), are asymmetric in every conformation, because the symmetry plane exchanging A and A* is destroyed by the biphenyl block B. However, unrestricted rotation between the blocks A and B on the one hand, and B and A* on the other hand, allows for the smooth interconversion between mirror-image conformers without involving achiral intermediates. Such molecules mimic, at the nanoscale level, the reversal of a real rubber glove by peeling it off inside out from the hand. At no time during the process of interconversion does the glove achieve a shape with a symmetry plane. Molecules mimicking this process have later on been coined "molecular rubber gloves." The chirality of *cis*-1,2-difluorohexane can be detected by ^{19}F NMR spectrometry at low temperature, where the exchange of mirror-image conformations through the achiral intermediate is blocked.

Molecular rubber-glove molecules are important milestones in stereochemistry, because they can be used as the basis to express the sufficient condition for chirality: if a molecule is chiral, then there are no enantiomerization chiral pathways converting an enantiomer into its mirror image [2].

1.2.2.2 Controlling Chirality by Coordination and Supramolecular Interactions

In this section we consider molecules that are not rigidly chiral but can exist in the form of enantiomeric conformations, which are in the fast exchange regime under observation conditions (stereochemical lability). Such molecules are interesting platforms to elicit

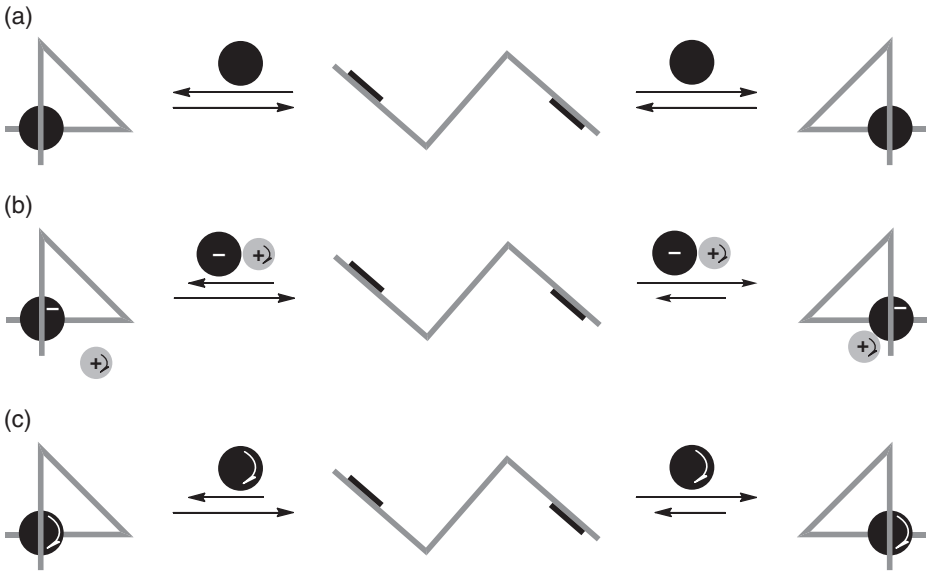

Figure 1.19 *Principle of freezing chirality by supramolecular or coordination interactions. A ditopic (black rectangles) linear receptor (central Z shape) can wrap around (a) an achiral guest (black disk) either clockwise (left) or anticlockwise (right). (b) If the guest is a charged species (e.g. an anion), the use of an optically active counter-ion (a cation) can lead to the control of host chirality by supramolecular ion-pair interactions. (c) The same result is obtained by using an optically active guest itself*

evidence of induced circular dichroism effects, to design chirality switches and molecular systems for chirality sensing (stereodynamic chemosensor), just to mention a few applications.

In order to control the chirality of a stereochemically labile molecule it is necessary to have an optically active chirality effector, which is able to interact with the former via supramolecular (e.g., hydrogen bonding, ion pair or van der Waals contact) or coordination interactions. Three cases of interest are reported schematically in Figure 1.19. Figure 1.19a represents the general case in which the achiral receptor, featuring two recognition elements, coils around an achiral guest. Assuming that the host-guest systems are in thermodynamic equilibrium, Figures 1.19b and 1.19c show two different approaches in order to control the sense of coiling of the host – either (Figure 1.19b) by using a ionic achiral guest in combination with an optically active counterion, or (Figure 1.19c) by using an optically active guest.

The phenomenon was independently described in the 1930s for the interaction of stereolabile transition metal complexes with optically active counterions by Pfeiffer [37] and Kuhn [38], who called it "asymmetric transformation." Most recent applications concern the design of receptors featuring chiral conformations, which can bind optically active guests. As a result, the dynamic equilibrium between diastereomeric host-guest pairs is biased towards the formation of the most stable one. Best evidence for the phenomenon was provided by induced circular dichroism. Figure 1.20 shows one of the numerous examples of the

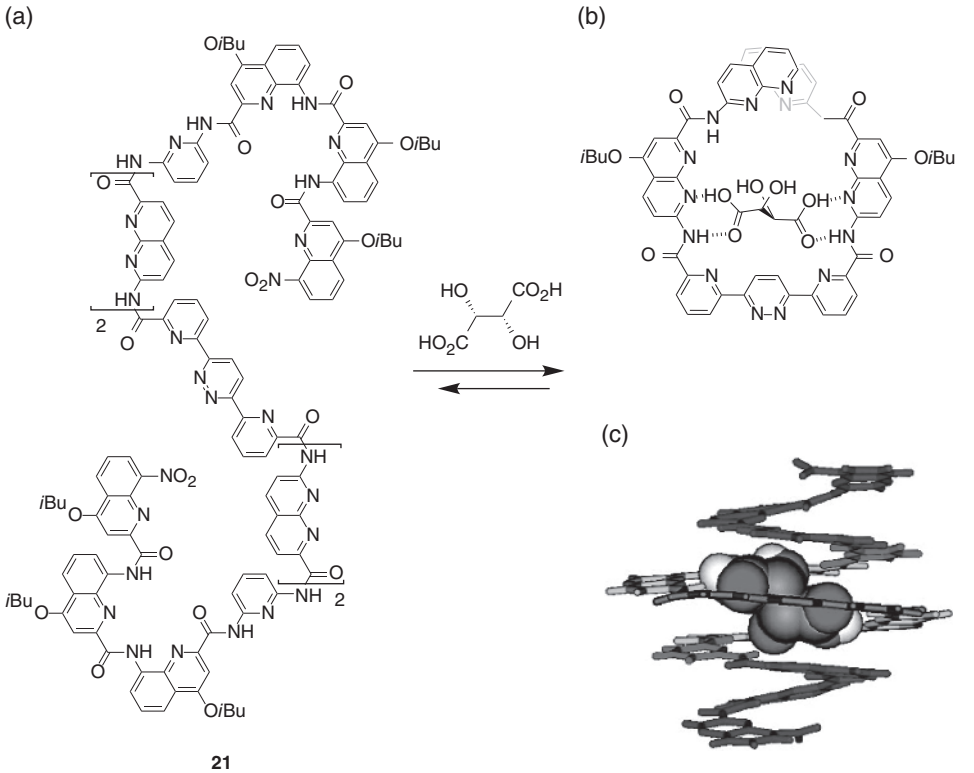

Figure 1.20 *Compound **21** (a), made of rigid aromatic hydrogen bond acceptors separated by carboxamide connectors, folds in a doubly conical, singly helical structure that features (b) a cavity able to host L-(+)-tartaric acid, as shown by (c) the view of the X-ray crystal structure. When the guest is optically pure, the diastereomeric purity of the host-guest ensemble is greater than 99%*

literature [39]. A foldamer (**21**) made of three different sequences symmetrically attached at the extremities of a central bis(pyridyl)pyridazine spacer forms a D_2-symmetrical bis-conical helical structure in $CHCl_3$/DMSO 98.8 : 0.2 v/v. This compact helical conformation features a central cavity, which is able to encapsulate various H-bond donor guests, such as L-(+)-threitol or L-(+)-tartaric acid (Figure 1.20). The latter, which shows the highest association constant ($5300\,M^{-1}$), also produces the stronger chiral bias, as the diastereomeric excess is greater than 99%.

1.2.2.3 Memory-of-Chirality Effects

Another related phenomenon is the "memory of chirality" effect, for which there has been evidence in the case of many achiral polymers that feature chiral helical conformations, such as polyacetylenes [40]. In addition, as we shall see in the next paragraph, this phenomenon is also frequently observed in the case of self-assembled helically chiral assemblies of molecules [41], but seldom in the case of small molecules. In the example

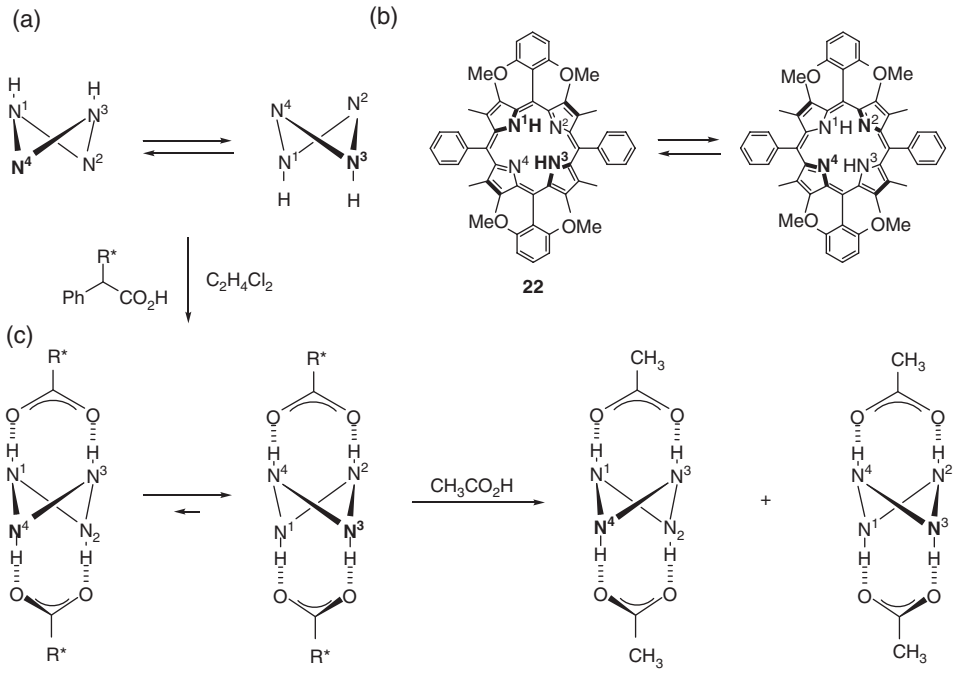

Figure 1.21 *Illustration of the chiral biasing of the equilibrium between mirror-image conformations of the ruffled porphyrin* ***22*** *depicted in (b). (a) Schematic view of the real system. (c) Addition of one equivalent of optically pure mandelic acid shifts the conformational equilibrium towards the formation of the most stable diastereomer. Replacement of mandelic acid by acetic acid, which is achiral, keeps the enantiomeric bias: this is the so-called memory-of-chirality effect*

shown in Figure 1.21 a sterically crowded porphyrin (**22**) has ruffled enantiomeric conformations in a 1 : 1 ratio. Binding of optically active carboxylic acid (host/guest = 1 : 2) by salt-bridge formation shifted the equilibrium to the most stable diastereomer (98% *de*), giving rise to an induced circular dichroism (ICD). Subsequently, the optically active carboxylic acid analyte was displaced by achiral acetic acid. The memory-of-chirality effect stems from the fact that there is no exchange between the acetic acid molecules bound to the hosts. As a consequence, two enantiomers (a major one and a minor one) are obtained. Remarkably, the ICD measured for the pair of enantiomers ($t_{1/2}$ = 200 h at 23 °C) is higher than the one measured for the pair of parent diastereomers [42].

Memory-of-chirality effects are actually more commonly observed in the case of chiral polymers. These are polymers taking up helical conformations, for example polyacetylenes, polyamides and polyisocyanates. Figure 1.22 shows schematically the experiments that could be carried out using a poly(aryl)acetylene carrying carboxylic acid functions [40]. The polymer takes up random-coil conformations that show domains with a well defined helical sense that are separated by reversal points. The polymer can be further functionalized by salt bridge formation with an optically active amine, which triggers the

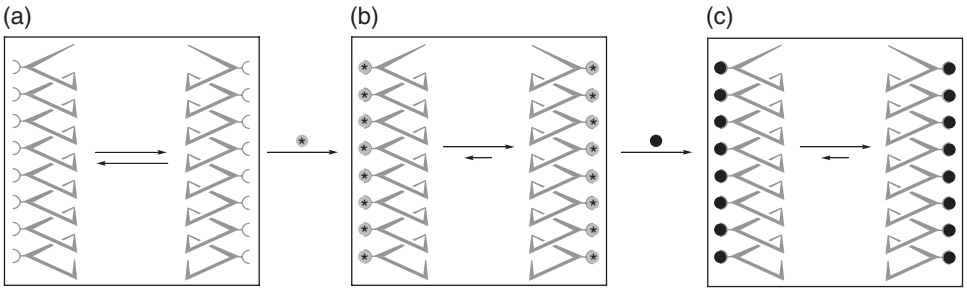

Figure 1.22 *Control of the chirality of polymers taking up helical conformations (a) by supramolecular interactions. The polymer contains appended binding groups, which upon interaction with a chiral, optically active guest (gray disks marked with a star), allow the control of the chiral bias between the mirror-image polymeric helices (b). (c) The memory-of-chirality effect takes place upon exchange of the chiral guest by an achiral analogue (black disks)*

homogenization of the favored chirality sense. The memory-of-chirality effect takes place upon exchange of the optically active amine for an achiral one.

1.2.2.4 Supramolecular Chirality

Supramolecular chirality must be distinguished from the previous cases, as it does not concern the chirality of an isolated molecule but the chirality of molecular assemblies constructed from achiral molecules held by noncovalent interactions (hydrogen bonding, coordination bonds, π-π stacking, dipole-dipole interactions, etc.) – such as aggregates of various shapes (in particular rods and ribbons), liquid crystals, solvent gels, and supramolecular polymers that are in dynamic equilibrium. The manifestation of supramolecular chirality is the formation of helical structures (see Figure 1.3), and these are characterized by circular dichroism. Remarkable phenomena have been observed (Figure 1.23). Chiral supramolecular polymers assembled from achiral molecular subunits (monomers) exist as racemates. Addition of an optically active chirality inducer (either a chiral version of the monomers, or a chiral molecule that is able to interact with the monomers) can bias the original equilibrium between the enantiomeric supramolecular polymers by formation of diastereomeric supramolecular polymers [41]. This phenomenon is a manifestation of the sergeant-and-soldiers principle, which was formulated for the first time in the case of covalent polymers made of achiral monomers plus a small amount of an optically active "dopant" [43]. The chiral "sergeant" molecule can be removed, without significantly altering the enantiomeric ratio between the mirror-image helices, because of kinetic effects. This is a manifestation, at the supramolecular level, of the memory-of-chirality effect [44].

Another chirality principle that was discovered in the case of covalent polymers, which also applies to supramolecular chirality, is the majority rule [45]. This rule applies when supramolecular polymerization uses only optically active chiral monomers. If an optically pure monomer is used, then an optically pure helical aggregate is obtained. However, if a racemate plus a slight excess of one of the enantiomer monomer is used, the majority rule tells us that the major supramolecular helical aggregate will be the one whose sense of chirality is dictated by the optically active monomer that is in excess [46].

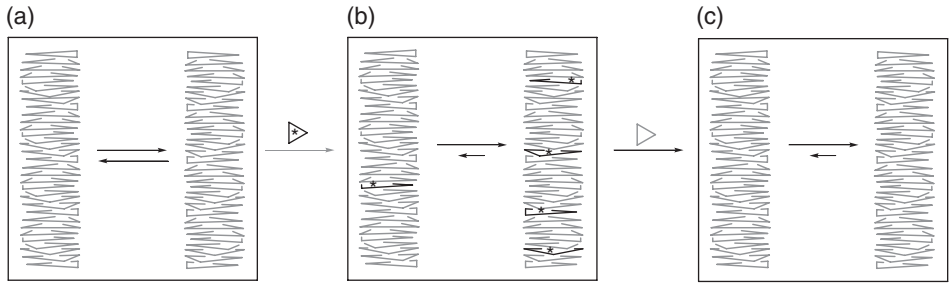

Figure 1.23 *Sergeant-and-soldiers principle in supramolecular chirality. (a) Aggregation of certain "soldier" achiral molecules (symbolized here as triangles) can lead to helical supramolecular structures held by π-π stacking or hydrogen bonding interactions. (b) Introduction of a small percentage of chiral, optically active monomer ("sergeant," starred triangle) leads to biasing of the ratio between the left- and right-handed supramolecular helices. (c) The "sergeant" molecules are replaced by equilibration with an excess of "soldier" molecules (grey triangle) without significantly changing the ratio between mirror-image stacks*

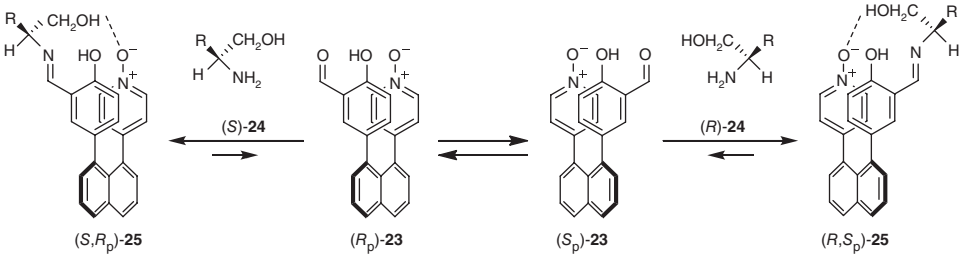

Figure 1.24 *A chemosensor (**23**) for chiral aminoalcohols based on a planar chiral naphthalene platform carrying a salicylaldehyde recognition subunit and a pyridine oxide chromophore*

1.2.2.5 Chirality Amplification and Switching of Chirality

The main consequence of dynamic chirality is the possibility of observing chirality amplification, because that chirality – be it of conformational or supramolecular origin – is never frozen once and for all. Chirality amplification translates into enhanced CD effects upon going from the optically active chirality inducer to the host-guest complex with the achiral receptor, because the latter may contain chromophores that are strongly CD active in a chiral environment [47]. As a consequence, the so-called induced circular dichroism (ICD) effect has been used as a principle of design for chirality sensors. Figure 1.24 shows one of numerous examples, in which a chiral aminoalcohol freezes out the enantiomeric conformations of a 1,8-diarylnaphthalene chromophore (**23**), by covalent and hydrogen bond formation between the analyte and the sensor [48]. In the case of supramolecular assemblies, positive nonlinear effects have been measured between the enantiomeric purity of the chiral dopant and the ICD of the assembly. Formation of supramolecular species (aggregates) could also explain nonlinear effects in asymmetric catalysis [49].

Chirality switching is not limited to molecular recognition and sensing. In some instances it has been induced by light irradiation [50] or solvent changes [51].

Finally, the phenomenon of supramolecular chirality resides at the interface between chirality at the nanometer level and chirality at the micrometer, if not millimeter, level. It is important to recall, in this respect, that it was the dissymmetric external shape of crystals of potassium tartrate examined with a microscope that suggested to Louis Pasteur that it could result from dissymmetric arrangements of the atoms of the salt. Hierarchical effects in chirality are observed in other materials than crystals. For example molecules forming liquid crystals can be combined with small amounts of chiral dopants that induce optically active liquid crystalline phases [52]. Similarly achiral molecular gelators can be doped with optically active analogs, leading to optically active solvent gels [53].

1.3 Topological Chirality

The chirality of a molecular object in the rigid geometry approximation is a property of the whole object, therefore it depends only on the positions of the atoms. This means that the bonds can be ignored, as first noted by Mislow [4]. This is exactly the opposite to the case of the topological character of chirality, which is invariant whatever the atomic positions, provided that all the connections (chemical bonds) between the atoms have been identified [3].

Molecular rigidity results from the stereochemical properties of atoms and bonds, from steric hindrance and strain, which limit the amplitude of bond rotations and elongations that could convert an enantiomer into its mirror image. It is at the very origin of geometrical chirality. There are cases, however, for which molecular rigidity is not a requirement for chirality, the molecule remaining chiral whatever the deformations – provided that no bonds can pass through each other. This is actually another form of molecular rigidity, which arises from topological constraints rather than geometrical ones. This section will focus on the concept of topological chirality, which, judging from the literature, has been somewhat overlooked.

1.3.1 The Molecular Graph

A graph G is an ordered pair (V, E) formed by a set of vertices V and a set of edges E connecting them. It is an abstract mathematical (topological) object; however, it can be embedded into and manipulated in 3D space. Whereas a geometrical figure is rigid and characterized by distances and angles, the embedded graph is endowed with complete flexibility: the vertices can be placed anywhere in space and the edges can be stretched or shrunk at will, the only requirement being that no two vertices can coincide and no two edges can cross each other – that is, edges and vertices represent boundaries that cannot be crossed. Embedded graphs in 3D space can be represented as a projection (the so-called presentation) in two dimensions, in which the relative positions of the projected edges (above or below) must be indicated [3]. Figure 1.25 shows different presentations of the $K_{3,3}$ graph, the so-called bipartite graph on three vertices, of which two are chiral. The topological property of $K_{3,3}$ is that it is a nonplanar graph – that is, it cannot be presented in the plane without any crossing. Examples of minimal presentations (a single crossing) are shown in Figure 1.25b and Figure 1.25c.

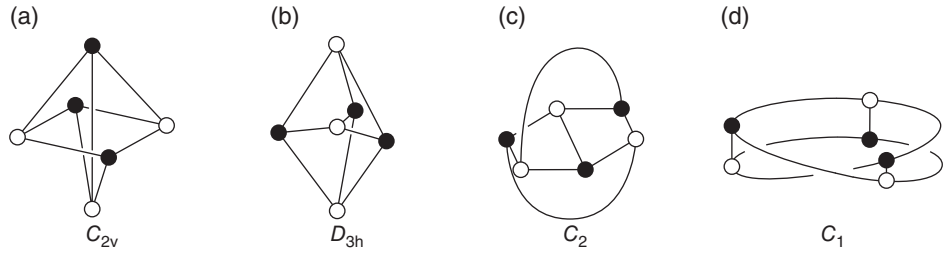

Figure 1.25 *Four presentations of the* $K_{3,3}$ *graph (the bipartite graph on three vertices) with their symmetry group. The presentations shown in (c) and (d) are geometrically chiral*

As the *graph of a molecule* is the set of atoms (vertices) and bonds (edges), it is equivalent to the molecular constitution. The *molecular graph* contains more information, because it has been defined as the embedded graph of a molecule, to take into account the fact that molecules are not abstract entities but real objects in 3D space [3, 4]. The molecular graphs of topological stereoisomers (including enantiomers) cannot be converted into each other by continuous deformations, whatever their amplitude. Walba, in his seminal paper about topological stereochemistry, defined an edge of the molecular graph to be a covalent bond and chose to leave open the question of a topologically significant bond. Topological stereoisomers are operationally distinct as long as, under the conditions of observation, the bonds involved in the graph are not labile – that is, cannot be broken and reformed [3].

Classical molecules exhibiting topological steroisomerism are those having the topology of knots and links [54]. Figure 1.26 shows the diagrams of the four first prime knots, including the unknot (a). The trefoil knot (b) has three crossings, the figure-of-eight knot (c) four, the pentafoil knot (d) five, etc. The simplest link is the Hopf link (f), which is made of a pair of singly interlocked rings. The Solomon link (g) is a pair of doubly interlocked rings. Of the links made from three subunits, the "Borromean rings" have a remarkable topology because they are formed from three interlocked rings that form disjointed pairs. Links and knots that have been realized chemically are the trefoil, the pentafoil, and the figure-of-eight knot on the one hand, and the Hopf and the Solomon links, and the "Borromean rings," on the other hand.

1.3.2 Topological Chirality

A chiral molecule is topologically chiral if and only if its enantiomers cannot be converted into each other by a continuous deformation [55, 56]. Such a property can be proved only by mathematical methods. On the other hand, topological achirality of a molecule is demonstrated by finding at least one achiral presentation of its molecular graph. For example, the trefoil knot has been shown to be topologically chiral, whereas the figure-of-eight knot is topologically achiral, because it has a S_4-symmetric presentation. However, the lack of the existence of at least one achiral presentation does not imply topological chirality, as exemplified by the so-called topological "rubber gloves" [57], which are topological analogs of the biphenyls mentioned in section 1.2.2.1.

The discovery that dynamic bonds (i.e., labile bonds that can be cleaved and reformed reversibly in certain conditions) can be used for the synthesis of topologically nonplanar molecules has opened a completely new field of investigations in molecular topology

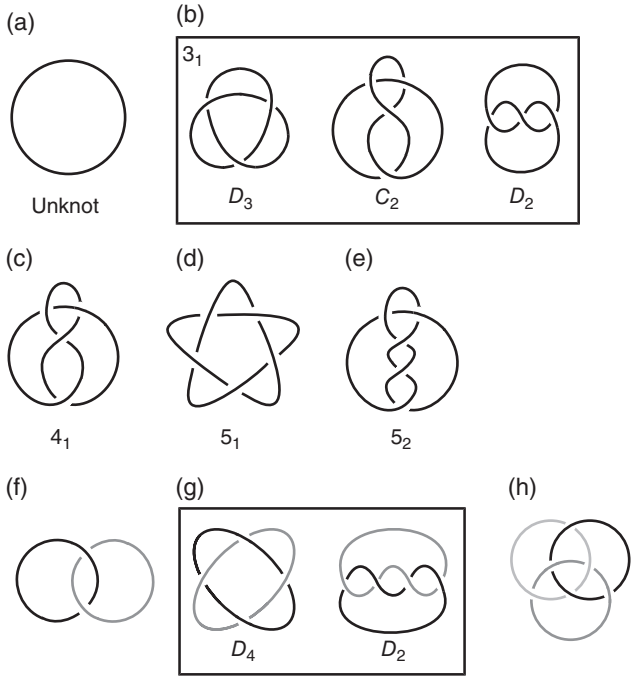

Figure 1.26 *Diagrams of the four first prime knots, (a) unknot, (b) 3_1 (trefoil knot, shown as its three common diagrams), (c) 4_1 (figure-of-eight knot; compare with the diagram of C_2 symmetry of 3_1), (d) 5_1 (pentafoil knot), (e) 5_2, (f) Hopf link, (g) Solomon link, (h) Borromean rings*

[58, 62]. Essentially, these bonds are either coordination bonds (e.g., palladium–nitrogen, gold–phosphorus), or covalent bonds (e.g., imine and disulfide being the most commonly used), and/or their combination (e.g., the formation of imine bonds under first-row transition metal templation). As the formation of these bonds operates under thermodynamic control, the reactions lead to mixtures of topological stereoisomers. *Sensu stricto*, only bonds that are not reversibly created and cleaved under the conditions of observation should be considered as topologically relevant, which limits them to classical covalent and some coordination bonds (those in the range above 30 kcal × mol^{-1}). In fact topological chirality can be considered from the formal or the operational viewpoint. Whereas the first case concerns the manipulation of graphs, the second concerns experiment. A molecule that is demonstrated to be topologically chiral based on a formal graph, may not be operationally (topologically) chiral because some of the bonds involved in the graph are reversible under the conditions of observation. Reciprocally, a molecule that is demonstrated to be chiral experimentally will obviously not be necessarily topologically chiral.

1.3.3 Topologically Relevant Molecules that are not Topologically Chiral

This section examines systems that are not topogically chiral, yet they have a nontrivial topology in relation to chirality. In fact they are topological analogues of the molecular rubber gloves discussed in section 1.2.2.1.

1.3.3.1 Topological Rubber-Glove Molecule

We have seen that a geometrical rubber-glove molecule was a molecule with a planar graph, which is rigidly chiral in all of its conformations, yet any conformation is converted into its mirror-image by a chemically realizable pathway, which means that no *meso* form is involved as intermediate in the conversion of a chiral conformer into its mirror-image enantiomer [3, 4]. To go a step further, a topological rubber-glove molecule adds to the definition above that it results from a graph embedding that has no planar presentation. It differs from the rubber glove itself, which could be physically stretched so as to bring it down to a simple flattened piece of rubber, thus making a real rubber glove an Euclidean rubber-glove. The concept of topological rubber-glove was illustrated by the [2]catenane shown in Figure 1.27 as its copper(I) complex (Cu**26**) [57]. This molecule is built from two different macrocycles based on the 2,9-diphenyl-1,10-phenanthroline chelate, one oriented by substitution of proton 4 by a *p*-tolyl group, the other incorporating a 1,5-binaphthol-derived fragment that is free to rotate about the aryl carbon-oxygen bonds. From the geometrical point of view the [2]catenane is chiral in all its conformations because the C_2-symmetry axis of the binaphthol-incorporating macrocycle, which is contained in the symmetry plane of the oriented macrocycle, cannot generate a second symmetry plane. However, the unhindered rotation of the binaphthol moiety allows the conversion of any conceivable conformation into its mirror image. As a consequence, the [2]catenane Cu**26** is not operationally chiral. However, as it cannot achieve any planar topological symmetry, it is a topological rubber glove.

1.3.3.2 The Figure-of-Eight Knot

The figure-of-eight knot is interesting for two reasons. Its classical presentation (diagram) is the one with rigid chiral C_2 symmetry, which must not be confused with the one of the trefoil knot (see Figures 1.26b and c). It is possible to convert the corresponding 3D structure into its mirror image by continuous deformation involving only chiral intermediates, which

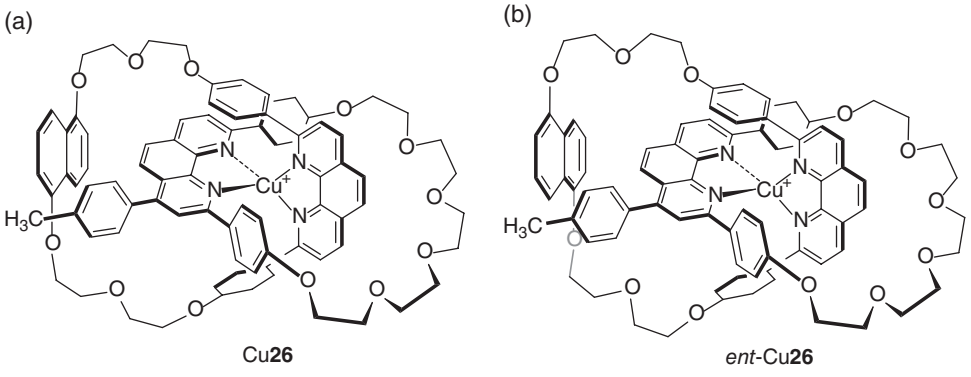

Figure 1.27 *A topological rubber glove molecule. The [2]catenane* ***26*** *represented as its copper(I) complex Cu****26*** *is chiral in all its conformations, but none of its presentations can be drawn in the plane without crossings, that is, has a symmetry plane. To convince the reader that (a) and (b) are indeed mirror images conformations, just rotate them in the plane by 90° clockwise. The mirror plane will appear in the middle*

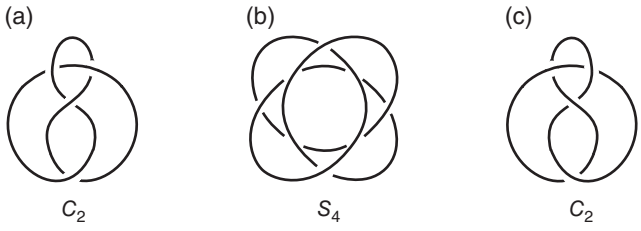

Figure 1.28 *Three diagrams of the figure-of-eight knot with their rigid symmetry point groups. Note that those shown in (a) and (c) are chiral and enantiomers of each other. The deformation pathway from one enantiomer to the other may involve only asymmetric presentations, which makes the corresponding transformation similar to that of an Euclidean rubber glove, however the existence of the* S_4*-symmetric presentation shown in (b), even if not attainable physically, precludes the figure-of-eight knot from being a topological rubber glove*

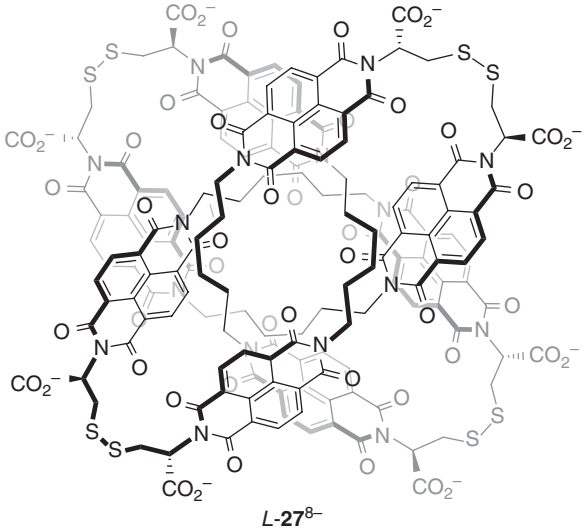

Figure 1.29 *Molecular structure of the water-soluble figure-of-eight knot* L-***27***$^{8-}$ *viewed as a rigidly chiral,* D_2*-symmetrical conformation*

makes the figure-of-eight knot appear at first glance as a topological rubber glove. However, it is also possible to draw a diagram of the figure-of-eight knot with an achiral S_4 symmetry (Figure 1.28b), which confirms that this knot is not chiral in all of its presentations and is therefore not topologically chiral, and that in addition it is not a topological rubber glove.

So far the only reported figure-of-eight knot (**27**$^{8-}$) was obtained, among other topological isomers (a doubly interlocked [2]catenane, and a trefoil knot), by dynamic covalent synthesis involving disulfide bond formation [62]. The reaction used a disulfide library generated from an optically active building block, a $(CH_2)_6$-bridged naphthalene diimide (NDI) dimer, the outer nitrogen atoms of which were functionalized with *L*-cysteine residues. The rigid, geometrically chiral D_2-symmetrical conformation of this molecule is shown in Figure 1.29, and was ascertained by ^{1}H NMR, mass spectrometry and circular

dichroism studies. The CD spectrum showed an intense negative couplet with an absolute maximum at 380 nm ($\Delta\varepsilon \sim -20 \times 10^4\,M^{-1}cm^{-1}$, water/acetonitrile, 75 : 25, v/v), which was independent of temperature and polarity, in agreement with the rigidly twisted character of the highly symmetric homochiral figure-of-eight knot. It must be stressed that if the carboxylate substituents were made planar (which is topologically allowed), the resulting molecule would have the topological achiral S_4-symmetry of diagram (b) of Figure 1.28.

Rather interestingly, a racemic library containing (*L*,*L*) and (*D*,*D*) naphthalene diimide (NDI) dimers led to the nearly exclusive formation (90%) of the *meso* form of the figure-of-eight knot. In principle, three diastereomers are possible, corresponding to the sequences *LL-DD-LL-DD*, *LL-LL-DD-DD*, and *LL-DD-DD-DD* of building blocks. However, only a single peak was observed by HPLC analysis, and ^{1}H NMR spectroscopy showed that the isolated compound exhibited twofold symmetry. This indicates that the *meso* figure-of-eight knot (*meso*-**27**$^{8-}$) is the *LL-DD-LL-DD* diastereomer, and that it exists as a mixture of mirror-image conformers having the geometrical C_2 symmetry, while the topological symmetry is S_4 (Figure 1.30). Quantitative 2D EXSY NMR showed that exchange between the latter had the following kinetic parameters: $\Delta H^{\ddagger} = -21\,kJ\,mol^{-1}$, $\Delta S^{\ddagger} = -302\,J\,K^{-1}\,mol^{-1}$, and $\Delta G^{\ddagger} = 69\,kJ\,mol^{-1}$ at 298 K, showing that it was controlled by entropy. This indicates that the transition state is highly destabilized, probably because the NDI hydrophobic surfaces, which are buried in the limiting conformers, are exposed to the aqueous solvent. Its diffusion coefficient is $2.0 \times 10^{-10}\,m^2/s$, which is slightly smaller than that of the homochiral figure-of-eight knot ($2.5 \times 10^{-10}\,m^2/s$). The ^{1}H NMR spectrum of the *meso* figure-of-eight knot shows sharper signals than its homochiral analogue, which was interpreted as the consequence of a perfect fit between its topological achirality and its *meso* character, whereas the latter is chiral from the geometrical viewpoint, yet it is topologically achiral.

1.3.4 Topologically Chiral Milestone Molecules (Based on Covalent Bonds)

1.3.4.1 Singly Interlocked [2]Catenanes

Catenanes are molecules made of two or more interlocking rings, and therefore they are the chemical realizations of the embedded graphs called links. The Hopf link, made of two interlocking rings, is the embedded graph of [2]catenanes. [2]Catenanes are topologically chiral if and only if they are made from oriented macrocycles – that is, macrocycles in which a bond sequence imparts an orientation [3].

1.3.4.1.1 From Copper(I) Templated Synthesis. The [2]catenanes shown in Figure 1.31a as their copper(I) complexes ([2]catenates) were the first of this type. Orientation is conferred to each macrocyclic polyether incorporating a 2,9-diphenyl-1,10-phenanthroline chelate, by aryl (phenyl in [Cu(**28**)]$^+$, *p*-tolyl in [Cu(**29**)]$^+$) substitution of the 4-position of the phenanthroline, making the resulting catenane C_2-symmetric [63, 64]. These compounds were synthesized as racemic copper complexes, and the corresponding catenanes were obtained by demetallation with cyanide. Partial analytical separation of the enantiomers of [Cu(**28**)](BF_4) was obtained by HPLC using amylose tris(3,5-dimethylphenylcarbamate)-coated silica gel and *n*-hexane/ethanol, 1 : 1 (v/v containing 0.1% of $LiPF_6$) as eluent. The first eluted enantiomer (70% ee) showed a positive Cotton effect centered around 340 nm, which corresponds to the MLCT band of the copper(I) complex. Its [α] was +1300° (ethanol, 0.015 g/L, 365 nm, 25 °C), quite comparable to the $[\alpha]_D$ of 1,3-diphenylallene,

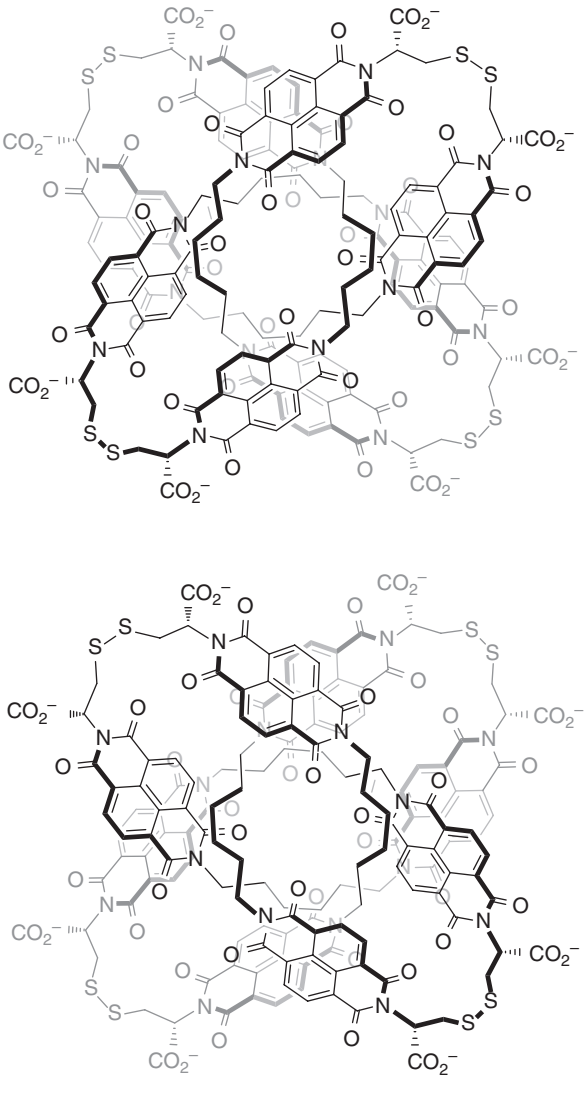

meso-**27**$^{8-}$

Figure 1.30 *Two mirror-image conformations of the achiral (*meso-***27**$^{8-}$*) figure-of-eight knot, which can be converted into each other by continuous deformation*

which has the same C_2-symmetry, and is a prototypical model of the chirality axis (see section 1.2.1 and Figure 1.7) [65].

1.3.4.1.2 From Hydrogen Bond Templated Synthesis. Other milestone examples of topologically chiral [2]catenanes are shown in Figure 1.31b. They were obtained by the amide bond formation method [66, 67]. These lactam-based catenanes differ from the earlier examples by the replacement of one of the four amide bonds by a sulfonamide bond

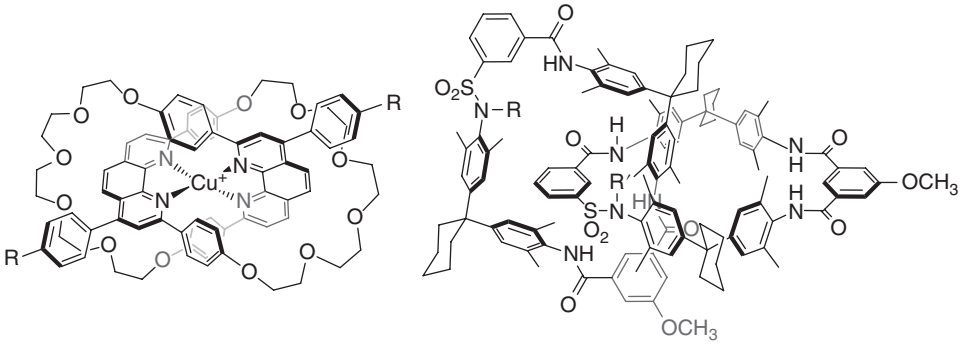

Figure 1.31 *Topologically chiral [2]catenanes. (a) Based on 2,9-diaryl-1,10-phenanthroline, as their copper(I) complexes, viewed along their C_2 symmetry axis. (b) From arylamide-based macrocycles incorporating one sulfonamide orientating group each*

in each macrocycle, which gives the latter an orientation that makes the corresponding catenanes topologically chiral. It must be noted that only a single conformer was obtained, the one in which the methoxy substituents display the *endo*/*exo* orientation, which renders these molecules asymmetric, contrary to the [2]catenanes of the previous section which are dissymmetric. The study of these asymmetrical catenanes (in terms of yield, conformation, X-ray crystal structure of racemic **32**) was very useful for establishing the mechanism of catenane formation via the "amide bond" formation. Catenanes **30** and **31** were resolved into their enantiomers by HPLC on Chiralcel OD column (eluent: hexane/2-propanol) with separation factors α of 6.95 and 2.39, respectively. (+)-**30** eluted at first, and showed an $[\alpha]_D$ value of 168° (compare with $[\alpha]_D = 282°$ measured in the same conditions for Tröger's base). The separated enantiomers of catenane **32** showed mirror-image CD spectra, with a strong couplet around 200 nm exhibiting large $\Delta\varepsilon$ values ($\pm$ 130 $M^{-1}cm^{-1}$) [68].

1.3.4.2 A Doubly Interlocked Catenane

Unlike singly interlocked [2]catenanes, doubly interlocked [2]catenanes, which are the chemical realization of the Solomon rings (or links), are unconditionally topologically chiral, because orientation of the rings is not necessary to make them dissymmetric. There are several examples of doubly interlocked [2]catenanes, the earliest being the one developed by the copper(I) phenanthroline template strategy.

The doubly interlocked [2]catenane, represented in Figure 1.32 as its tri-copper(I) complex ($[Cu_3\mathbf{33}]^{3+}$), belongs to a family of compounds that differ by the nature of the bridges between the phenanthroline subunits [69, 70]. Its high yield synthesis relied on the successful formation of an unusual trinuclear double-helical complex of Li^+ with two phenanthroline-based tri-chelate ligands, in order to achieve the presentation of D_2 symmetry shown in Figure 1.26g, and on the use of ring closing alkene metathesis as "topologically fixing" step [71]. It was, however, purified as its tri-copper(I) complex obtained by transmetallation.

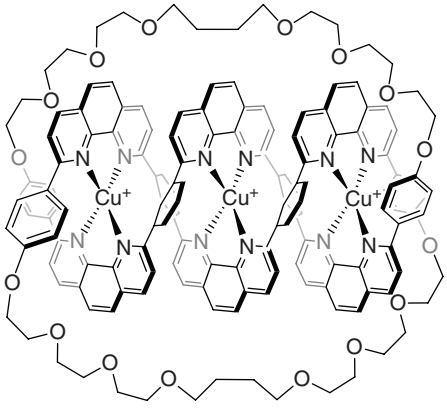

$[Cu_3(\mathbf{33})]^{3+}$

Figure 1.32 *A topologically chiral doubly interlocked [2]catenane ($[Cu_3\mathbf{33}]^{3+}$) based on copper(I) phenanthroline complex subunits. The view is shown along one of its three C_2-symmetry axes*

The metal-free doubly interlocked [2]catenane **33** was obtained quantitatively by treatment with an excess of potassium cyanide in acetonitrile, and was characterized by an ^{1}H NMR spectrum exhibiting broad features, thus pointing to restricted intramolecular motions occurring at the NMR timescale.

1.3.4.3 Molecular Knots

Since the pioneering work of Sauvage, Buchecker, and coworkers, several examples of molecular trefoil knots have been published. They have been synthesized according to various strategies [71]. It is noteworthy that the transition metal approach has used the three presentations shown in Figure 1.26b. This short review will be restricted to examples of molecular trefoil knots that were resolved into their enantiomers.

1.3.4.3.1 Trefoil Knots from Double-helical Precursors. This trefoil knot is a typical example of a trefoil knot, the construction of which follows a predicted sequence (kinetic template). The synthesis of this trefoil knot relied on the successful stabilization of a dinuclear double-helical complex of copper(I) with two 2,9-diphenyl-1,10-phenanthroline (dpp)-based di-chelate ligands, in order to achieve the presentation of D_2 symmetry shown in Figure 1.26b. In earlier syntheses, the chiral trefoil knot $[Cu_2(\mathbf{k\text{-}86})]^{2+}$ and the *meso* face-to-face complex $[Cu_2(\mathbf{m\text{-}43})_2]^{2+}$ were formed (Figure 1.33), however they could not be differentiated by standard ^{1}H NMR, as they both showed diastereotopic pairs of protons [72]. Internal correlation times for the protons of the central -$(CH_2)_4$- bridge were longer in the case of the knotted system by comparison with the other, pointing to a significant decrease of mobility of this methylenic chain in the case of the knot. The connection of the two phenanthroline subunits by a *meta*-phenylene spacer rather than a -$(CH_2)_n$- chain turned out to be crucial, as

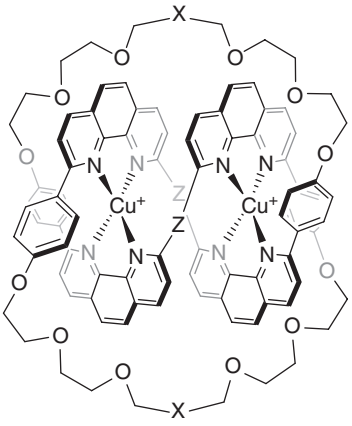

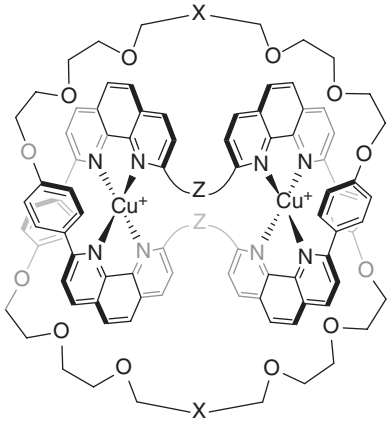

$[Cu_2(\mathbf{k\text{-}80})]^{2+}$: X = /, Z = $(CH_2)_4$
$[Cu_2(\mathbf{k\text{-}82})]^{2+}$: X = CH_2OCH_2, Z = $(CH_2)_2$
$[Cu_2(\mathbf{k\text{-}83})]^{2+}$: X = $(CH_2)_2$, Z = *m*-C_6H_4
$[Cu_2(\mathbf{k\text{-}84})]^{2+}$: X = /, Z = $(CH_2)_6$
$[Cu_2(\mathbf{k\text{-}85})]^{2+}$: X = CH_2OCH_2, Z = *m*-C_6H_4
$[Cu_2(\mathbf{k\text{-}86})]^{2+}$: X = CH_2OCH_2, Z = $(CH_2)_4$
$[Cu_2(\mathbf{k\text{-}90})]^{2+}$: X = CH_2OCH_2, Z = $(CH_2)_6$

$[Cu_2(\mathbf{m\text{-}40})_2]^{2+}$: X = /, Z = $(CH_2)_4$
$[Cu_2(\mathbf{m\text{-}41})_2]^{2+}$: X = CH_2OCH_2, Z = $(CH_2)_2$
$[Cu_2(\mathbf{m\text{-}42})_2]^{2+}$: X = /, Z = $(CH_2)_6$
$[Cu_2(\mathbf{m\text{-}43})_2]^{2+}$: X = CH_2OCH_2, Z = $(CH_2)_4$
$[Cu_2(\mathbf{m\text{-}45})_2]^{2+}$: X = CH_2OCH_2, Z = $(CH_2)_6$

Figure 1.33 *Structural formulae of trefoil molecular knots synthesized via the copper(I)-templated strategy and the corresponding face-to-face complexes. The numbers following k (for knot) and m (for macrocycle) correspond to the minimum number of atoms in each macrocycle*

it allowed for the transition metal-templated synthesis of the trefoil knot $[Cu_2(\mathbf{k\text{-}85})]^{2+}$ in significantly improved yield (29%), without the observation of face-to-face complex formation. In its most accomplished version, the cyclization reaction involved alkene metathesis and the yield of the corresponding knot $[Cu_2(\mathbf{k\text{-}83})]^{2+}$ was raised to 74%. The metal-free knots were obtained as metal-free catenanes by competitive reaction with cyanide.

Very gratifyingly, the di-copper complex of the trefoil knot $[Cu_2(\mathbf{k\text{-}86})]^{2+}$ crystallized as a conglomerate of enantiomers, therefore exhibiting spontaneous resolution [73]. However the first planned resolution of a molecular trefoil knot was performed by separation of ion-pair diastereomeric derivatives [74]. The knot $[Cu_2(\mathbf{k\text{-}85})]^{2+}$, one enantiomer of which is illustrated in Figure 1.34a, is a dication and its diastereomeric salt with the (+)-(*R*)-binaphthylphosphate (BNP) optically active anion was formed by anion exchange followed by fractional crystallization. This allowed for the resolution of the di-copper(I) complex into optically pure crystalline [(+)-(*M*)-$Cu_2(\mathbf{k\text{-}85})$]·2[(+)-(*R*)-$BNP^-$], while optically pure [(–)-(*P*)-$Cu_2(\mathbf{k\text{-}85})$]·2[(+)-(*R*)-$BNP^-$] could be isolated from a mother liquor. After exchange of [(+)-(*R*)-BNP^-] back for PF_6^-, the chiroptical properties of the resolved complexes were measured, and the circular dichroism spectrum was shown to exhibit pronounced Cotton effects. The $\Delta\varepsilon$ value reached a maximum of $\pm 20.7\,M^{-1}cm^{-1}$ in the visible, corresponding to the absorption maximum of the MLCT transition at 510 nm. The molar rotation $[M]_D$ was +73000 for [(+)-(*M*)-$Cu_2(\mathbf{k\text{-}85})$] $(PF_6)_2$.

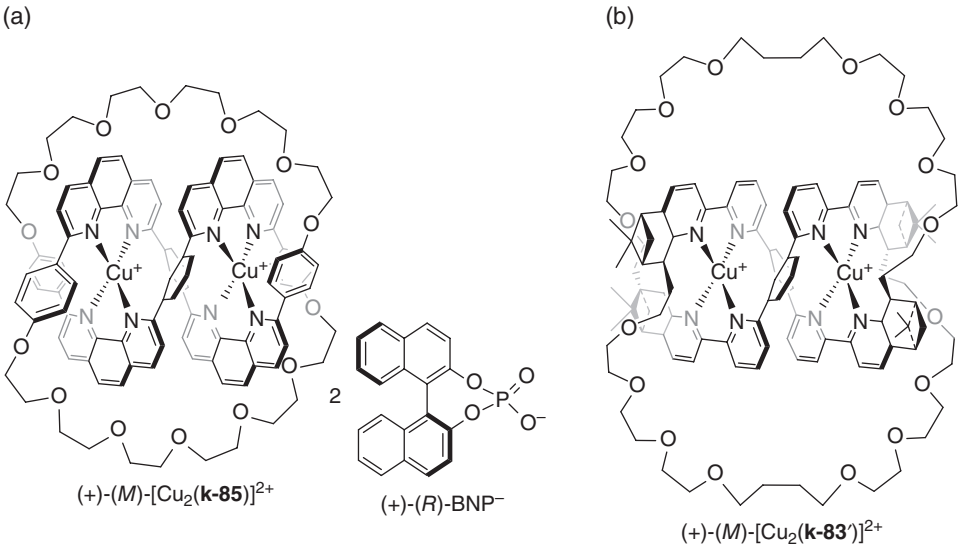

Figure 1.34 *Topologically chiral trefoil molecular knots based on large ring macrocycles incorporating four chelates derived from dpp ([Cu_2(**k-85**)]$^{2+}$, left) or bipy (Cu_2(**k-83′**)]$^{2+}$, right), shown as their D_2-symmetric bis-copper(I) complexes with M helicity. Attached to the [(+)-(M)-Cu_2(**k-85**)$^{2+}$] dication is the [(+)-(R)-BNP$^-$] optically active anion that was used for its resolution by fractional crystallization*

As an alternative, a related trefoil knot was obtained by stereoselective synthesis. Indeed, the use of enantiomerically pure di-chelate ligands (obtained by constructing (+)-(*R*)-α-pinene-fused 2,2′-bipyridyl ligands belonging to the so-called CHIRAGEN family), led to the stereoselective formation of the di-copper double helix having the *M* absolute configuration, as shown by a positive exciton couplet [75]. This helicity was further transferred to the knotted system ([Cu_2(**k-83'**)]$^{2+}$), which was obtained in 74% isolated yield by ring-closing metathesis reaction followed by a quantitative catalytic hydrogenation (Figure 1.34b).

The metal-free knots retain high molar rotations (e. g., +20000 for [(+)-(*M*)-(**k-85**)]), which are comparable to values found in the case of helicenes. The ^{1}H NMR spectrum of the molecular knot **k-84** in d^7-DMF shows broad features at room temperature, indicative of molecular motions that could be identified to a molecular "reptation" phenomenon. Variable temperature studies gave a ~2 s characteristic time for these motions. Upon heating the solution of the knot, a well resolved spectrum is obtained, which shows that the two phenanthroline subunits are again equivalent, as in the di-copper complex. A process of conformational change that has been called "reptation" allows all the atoms to occupy all the possible positions along the molecular knot **k-84**, which achieves in such a way the maximal topological D_3 symmetry. Interestingly, this latter symmetry is clearly apparent in the atomic force microscopy (AFM) image of a trefoil knotted polymer synthesized via ring expansion of a Sn(IV)-locked molecular knot precursor displaying the D_2 symmetry [76].

1.3.4.3.2 Trefoil Knots Based on Hydrogen Bonding Interactions. These trefoil knots are an illustration of systems obtained by serendipity (Figure 1.35). The first "knotane"

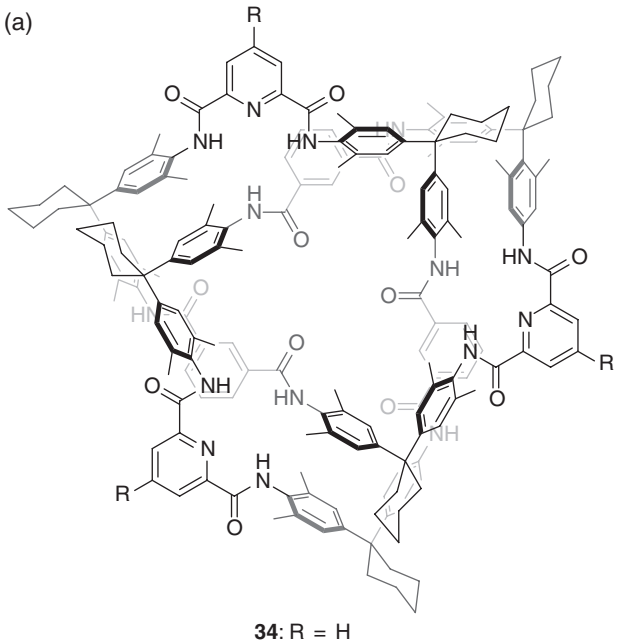

34: R = H
35: R = O-allyl

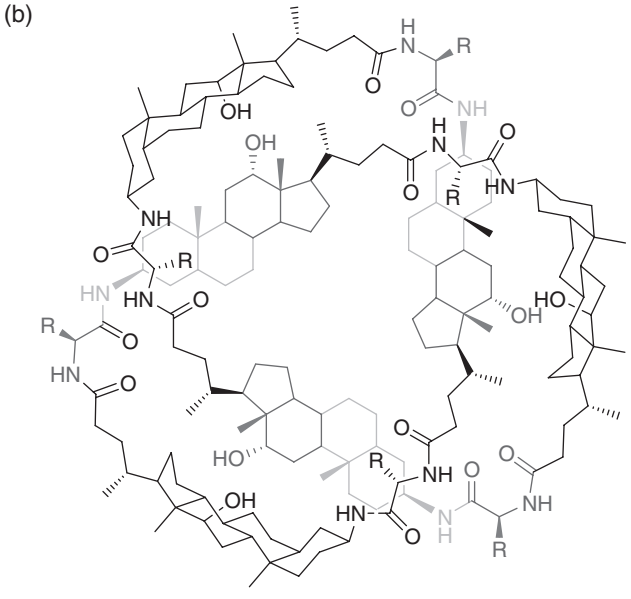

36

Figure 1.35 *Trefoil knots based on hydrogen bonding and other interactions. (a) General structure of amide-based knotanes:* ***34*** *(R=H) is the first member of a series of compounds;* ***35*** *(R=OCH_2CHCH_2=O-allyl) is the knotane that was used for further functionalization. (b) General structure of knots* ***36*** *based on optically active choline spacers between dipeptide fragments*

(**34** of Figure 1.35a) was obtained in the course of the synthesis of rigid macrocycles incorporating 2,6-pyridine and 1,3-benzenedicarboxamide subunits as precursors of catenanes. Corresponding to the knotted macrocyclic trimer, it was isolated in 20% yield alongside with the target large ring macrocyclic dimer (23%) and the macrocyclic monomer (20%) [77]. An X-ray crystal structure analysis of racemic crystals of knotane **34** showed that there were four intramolecular hydrogen bonds, and that the molecular structure had C_1 symmetry. This was confirmed in solution at the NMR timescale by the study of a more soluble analogue, knotane **35** (Figure 1.35a), in which $R = OCH_2CHCH_2$ (O-allyl). In $CDCl_3$, the ^1H NMR spectrum showed very broad features, pointing to the occurrence of conformational changes taking place at the NMR timescale. However, these were slowed either by cooling down the solution to 223 K, or by adding 10% d^6-DMSO at room temperature (and of course in pure d^6-DMSO at RT). Both experiments afforded a well resolved ^1H NMR spectrum corresponding to a C_1-symmetric species.

Knotane **34** was resolved on a Chiralpak-AD HPLC column using a mixture of *n*-hexane/$CHCl_3$/iPrOH, 30 : 20 : 1, v/v as eluent, with a large separation factor ($\alpha = 2.14$) [78]. The experimental CD spectra showed mirror image curves for the (+) and (−) enantiomers, with maxima at 240 nm ($\Delta\varepsilon = +100/-108\,M^{-1}cm^{-1}$), 272 nm ($\Delta\varepsilon = \pm 4\,M^{-1}cm^{-1}$), and 293 nm ($\Delta\varepsilon = \pm 8\,M^{-1}cm^{-1}$). The strong band at 240 nm, which results mainly from exciton-coupled $B_{a/b}$ states of the benzene/benzene-amide subunits, was stable with respect to variations in the calculations and could be used to assign the absolute configuration of the levorotatory enantiomer at 365 m, which showed a negative Cotton effect at 240 nm, as the (*P*,*P*,*P*) one.

The second case (**36**, Figure 1.35b) represents another example of the stereoselective synthesis of a molecular knot [79]. With the aim of obtaining macrolactams incorporating the choline scaffold, a linear trimeric aminoacid incorporating three choline fragments was subjected to peptide bond formation conditions. The desired macrocycle was obtained in 31% yield, and significant amounts (21% yield) of a compound were isolated that could be identified as a trefoil knot macrocycle incorporating six choline subunits (Figure 1.35b). The knotted nature of the system was identified without any ambiguity by an X-ray crystal structure analysis, which showed the threefold symmetry of the molecule and that the chirality of the starting aminoacid was fully transferred to the knot, which exhibited the *P* helicity. It is noteworthy that the molecular knot showed enhanced CD properties by comparison with the cyclic analogue, as its normalized Θ value (48 000° at 200 nm) was nearly five times higher.

1.3.4.3.3 A Pentafoil Knot from a Circular Helicate. Just as binuclear double helicates were found to be ideal precursors for the trefoil knot, pentanuclear circular helicates were used as precursors for the pentafoil knot. Lehn and coworkers had shown that a linear tris(2,2′-bipyridyl) molecular fragment (**37**) with short connections (ethylene linkers) between the central and the peripheral chelates favored the formation of the circular pentafoil pentanuclear helicate $[Fe_5(\mathbf{37})_5]^{10+}$ with respect to the corresponding linear triple-stranded trinuclear helicate in the presence of Fe^{2+} cations, and a chloride anion – which played the role of template (Figure 1.36a) [80]. Subsequently, Leigh and coworkers were able to show that the same kind of assembly could be obtained if the peripheral bipyridyl subunits were replaced by α-imino pyridyl chelates generated during the assembly process from a molecular thread incorporating a central bipyridyl subunit and 2-pyridylcarboxaldehyde end groups, and various aliphatic amines [81]. The use of enantiomerically pure

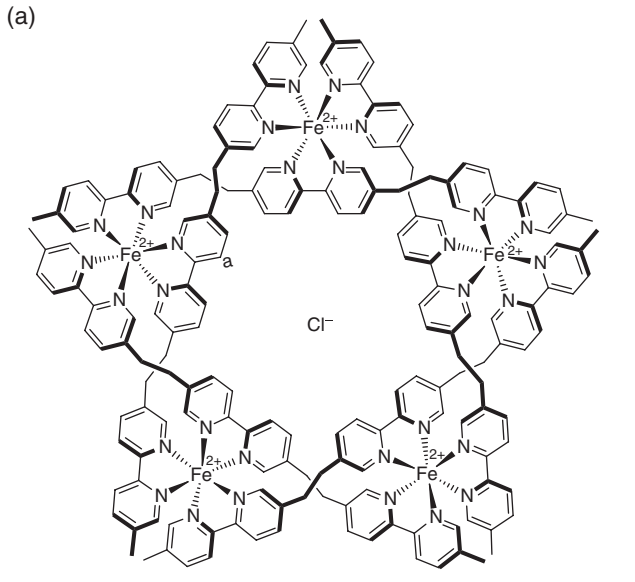

$[Fe_5(\mathbf{37})_5]^{10+} \supset Cl^-$

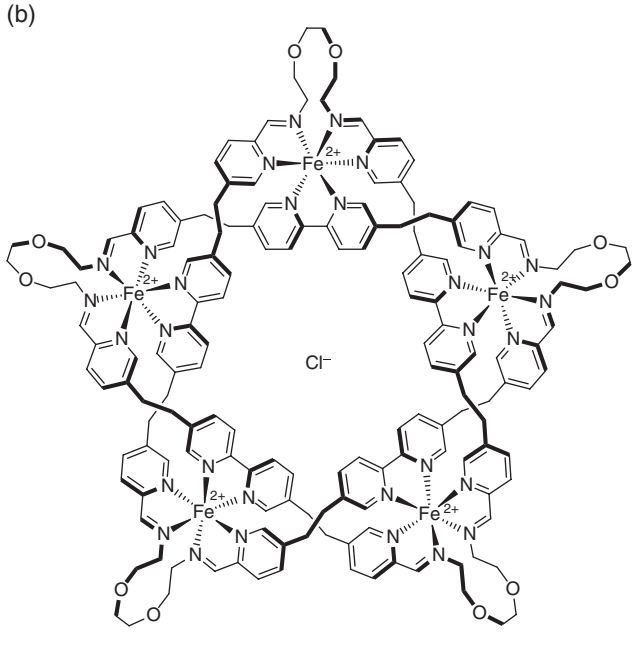

$[Fe_5(\mathbf{38})]^{10+} \supset Cl^-$

Figure 1.36 *(a) The original circular pentanuclear Fe^{2+} helicate $[Fe_5(\mathbf{37})_5]^{10+}$ as its chloride complex. (b) A pentafoil molecular knot $[Fe_5\mathbf{38}]^{10+}$ based ion a circular pentanuclear Fe^{2+} helicate precursor*

amines led to the complete control of the helical sense of the circular helicate, as demonstrated by circular dichroism studies. Thanks to the fact that the two terminal alkyl imines are close to each other (template effect), intramolecular bridging by using a diamine was envisaged in order to connect the five tri-chelate molecular threads so as to generate *in situ* a pentafoil knotted giant macrocycle. Simple alkyl chain diamines gave complex mixtures of oligomers but the use of the diamine deriving from triethylene glycol afforded the desired pentafoil knot $[Fe_5\mathbf{38}]^{10+}$ after two days reaction in 44% isolated yield (Figure 1.36b). The chirality and symmetry of the pentafoil knot were analyzed by ^{1}H NMR spectroscopy, which showed the presence of diastereotopic pairs of methylene protons, and by X-ray crystallography, which brought a definitive proof of the topology of the molecule. Removal of the chloride anion by treatment with a large excess of $AgPF_6$ produced the chloride-free trefoil knot, however no attempts were made to remove the templating metal cations.

1.4 Conclusion

Chirality, the nonsuperimposability of a molecular object or assembly with its mirror image, is one of the most ancient concepts of chemistry. However, in spite of its apparent simplicity it underlies many difficulties. These are principally due to the fact that molecules are complex nanoscale objects that cannot be described by a single model. We have shown that, starting from an achiral object, chirality arises either from a constitutional change or a twist, or both. The most significant advances in recent decades are the synthesis and resolution of topologically chiral molecules (in particular trefoil knots), and developments in the supramolecular transfer of chirality and the supramolecular chirality itself, which are strongly interconnected. Whereas the former explains effects as different as enantioselective catalysis by transition metals and organocatalysis, enantiomeric resolution and chirality detection by ICD effects, the latter has led to the development of chiral materials that have made molecular chirality tangible at the macroscopic level, as foreseen by Louis Pasteur.

References

[1] Liang, C., Mislow, K. (1994) Classification of topologically chiral molecules. *J. Math. Chem.*, **15** (1), 245–260.
[2] For an account on the historical development of chirality, see: O'Loane, J. K. (1980) Optical activity in small molecules, nonenantiomorphous crystals, and nematic liquid crystals. *Chem. Rev.*, **80** (1), 41–61.
[3] Walba, D. M. (1985) Topological stereochemistry. *Tetrahedron*, **41** (16), 3161–3212.
[4] Mislow, K. (1999) Molecular chirality. *Top. Stereochem.*, **22**, 1–82.
[5] Mislow, K., Bickart, P. (1976/1977) An epistemological note on chirality. *Isr. J. Chem.*, **15** (1–2), 1–6.
[6] Hasenknopf, B., Micoine, K., Lacôte, E., *et al.* (2008) Chirality in polyoxometallate chemistry. *Eur. J. Inorg. Chem.*, **32**, 5001–5013.
[7] Tsuda, A., Kakamura, T., Sakamoto, S., *et al.* (2002) A self-assembled porphyrin box from *meso-meso* linked bis{5-*p*-pyridyl-15-(3,5-di-octyloxyphenyl)porpyrinato zinc(II)}. *Angew. Chem. Int. Ed.*, **41** (15), 2817–2821.
[8] Cahn, R. S., Ingold, C., Prelog, V. (1966) Specification of molecular chirality. *Angew. Chem. Int. Ed.*, **5** (4), 385–415.
[9] Prelog, V. (1976) Chirality in chemistry. *Science*, **193** (4247), 17–24.
[10] Danjo, H., Iwaso, K., Kawahata, M., *et al.* (2013) Preparation of tris(spiroorthocarbonate) cyclophanes as back to back ditopic hosts. *Org. Lett.*, **15** (9), 2164–2167.

[11] Yashima, E. (2010) Synthesis and structure determination of helical polymers. *Polymer J.*, **42** (1), 3–16.
[12] Guichard, G., Huc, I. (2011) Synthetic foldamers. *Chem. Commun.*, **47**, 5933–5941.
[13] Gingras, M. (2013) One hundred years of helicene chemistry. Part 1: non-stereoselective syntheses of carbohelicenes. *Chem. Soc. Rev.*, **42**, 968–1006.
[14] Provent, C. and Williams, A. (1999) The chirality of polynuclear transition metal complexes, in *Transition Metals in Supramolecular Chemistry* (ed. J.-P. Sauvage), John Wiley & Sons, Ltd, Chichester, pp. 135–192.
[15] Laleu, B., Bernardinelli, G., Chauvin, R., Lacour, J. (2006) Trimesitylmethylphosphonium cation. Supramolecular stereocontrol and simple enantiomerization mechanism determination. *J. Org. Chem*., **71** (19), 7412–7416.
[16] Glasson, C. R. K., Meehan, G. V., Clegg, J. K., *et al.* (2008) Microwave synthesis of a rare $[Ru_2L_3]^{4+}$ triple helicate and its interaction with DNA. *Chem. Eur. J.*, **14** (34), 10535–10538.
[17] Bassani, D., Lehn, J.-M., Fromm, K., Fenske, D. (1998) Toposelective and chiroselective self-assembly of [2×2] grid-type inorganic arrays containing different octahedral metallic centers. *Angew. Chem. Int. Ed.*, **37** (17), 2364–2367.
[18] Anet, F. A. L., Miura, S. S., Siegel, J., Mislow, K. (1983) La coupe du roi and its relevance to stereochemistry. Combination of two homochiral molecules to give an achiral product. *J. Am. Chem. Soc.*, **105** (6), 1419–1426.
[19] Thilgen, C., Herrmann, A., Diederich, F. (1997) Configurational description of chiral fullerenes and fullerene derivatives with a chiral functionalization pattern. *Helv. Chim. Acta*, **80** (1), 183–199.
[20] Szumna, A. (2010) Inherently chiral concave molecules – from synthesis to applications. *Chem. Soc. Rev.*, **39**, 4274–4285.
[21] Wang, T., Zhang, Y.-F., Hou, Q.-Q., *et al.* (2013) C_3-symmetrical tribenzotriquinacene derivatives: Optical resolution through cryptophane synthesis and supramolecular self-assembly into nanotubes. *J. Org. Chem.*, **78** (3), 1062–1069.
[22] Higashibayashi, S., Sakurai, H. (2008) Asymmetric synthesis of a chiral buckybowl, trimethylsumanene. *J. Am. Chem. Soc.*, **130** (27), 8592–8593.
[23] Sánchez-Molina, I., Grimm, B., Calderon, R. M. K., *et al.* (2013) Self-assembly, host-guest chemistry, and photophysical properties of subphthalocyanin-based metallo-supramolecular capsules. *J. Am. Chem. Soc.*, **135** (28), 10503–10511.
[24] Brotin, T., Dutasta, J.-P. (2009) Cryptophanes and their complexes – present and future. *Chem. Rev.*, **109** (1), 88–130.
[25] Vysotsky, M. O., Pop, A., Broda, F., *et al.* (2001) Molecular motions within self-assembled dimeric capsules with tetraethylammonium cations as guest. *Chem. Eur. J.*, **7** (20), 4403–4410.
[26] Dalla Cort, A., Mandolini, L., Pasquini, C., Schiaffino, L. (2004) "Inherent chirality" and curvature. *New J. Chem.*, **28**, 1198–1199.
[27] Lukášek, J., Böhm, S., Dvořáková, H., *et al.* (2014) Regioselective halogenation of thiacalix[4] arenes in the cone and 1,3-alternate conformations. *Org. Lett.*, **16** (19), 5100–5103.
[28] Collet, A., Gabard, J., Jacques, J., *et al.* (1981) Synthesis and absolute configuration of chiral (C_3) cyclotriveratrylene derivatives. Crystal structure of (*M*)-(–)-2,7,12-triethoxy-3,8,13-tris-[(*R*)-1-methoxycarbonylethoxy]-10,15-dihydro-5*H*-tribenzo[a,d,g]-cyclononene. *J. Chem. Soc., Perkin Trans.* 1, 1630–1638.
[29] Guieu, S., Zaborova, E., Blériot, Y., *et al.* (2010) Can hetero-polysubstituted cyclodextrins be considered as inherently chiral concave molecules ? *Angew. Chem. Int. Ed.*, **49** (13), 2314–2318.
[30] Sendhoff, N., Weissbarth, K.-H., Vögtle, F. (1987) Synthesis and chirality of sixfold-bridged triple-decker phanes. *Angew. Chem. Int. Ed. Engl.*, **26** (8), 777–779.
[31] Hasenknopf, B., Lehn, J.-M., Kneisel, B. O., *et al.* (1996) Self-assembly of a circular double helicate. *Angew. Chem. Int. Ed.* **35** (16), 1838–1840.
[32] Yeh, R. M., Xu, J., Seeber, G., Raymond, K. N. (2005) Tetrahedral coordination cages: an extension of symmetry-based design. *Inorg. Chem.*, **44** (18), 6228–6239.
[33] Meng, W., Clegg, J. K., Thoburn, J. D., Nitschke, J. R. (2011) Controlling the transmission of stereochemical information through space in terphenyl-edged Fe_4L_6 cages. *J. Am. Chem. Soc.*, **133** (34), 13652–13660.

[34] Prince, R. B., Barnes, S. A., Moore, J. S. (2000) Foldamer-based molecular recognition. *J. Am. Chem. Soc.*, **122** (12), 2758–2762.
[35] Shi, Z.-M., Chen, S.-G., Zhao, X., *et al.* (2011) *meta*-substituted benzamide oligomers that complex mono-, di- and tricarboxylates: folding-induced selectivity and chirality. *Org. Biomol. Chem.*, **9**, 8122–8129.
[36] Mislow, K., Bolstad, R. (1955) Molecular dissymmetry and optical inactivity. *J. Am. Chem. Soc*., **77** (24), 6712–6713.
[37] Pfeiffer, P., Quehl, K. (1931) Über einen neuen Effekt in Lösungen optisch-aktiver Substanzen. *Chem. Ber.*, **64** (10), 2667–2671.
[38] Kuhn, R. (1932) Über einen neuen Effekt in Lösungen optisch-aktiver Substanzen. *Chem. Ber.*, **65** (1), 49–51.
[39] Ferrand, Y., Kendhale, A. M., Kauffmann, B., *et al.* (2010) Diastereoselective encapsulation of tartaric acid by a helical aromatic oligoamide. *J. Am. Chem. Soc.*, **132** (23), 7858–7859.
[40] Maeda, K., Morino, K., Okamoto, Y., *et al.* (2004) Mechanism of helix induction on a stereoregular poly((4-carboxyphenyl)acetylene) with chiral amines and memory of the macromolecular helicity assisted by interaction with achiral amines. *J. Am. Chem. Soc.*, **126** (13), 4329–4342.
[41] Helmich, F., Lee, C. C., Schenning, A. P. H. J., Meijer, E. W. (2010) Chiral memory via chiral amplification and selective depolymerization of porphyrin aggregates. *J. Am. Chem. Soc.*, **132** (47), 16753–16755.
[42] Mizuno, Y., Aida, T., Yamaguchi, K. (2000) Chirality-memory molecule: Crystallographic and spectroscopic studies on dynamic molecular recognition events by fully substituted chiral porphyrins. *J. Am. Chem. Soc.*, **122** (22), 5278–5285.
[43] Green, M. M., Peterson, N. C., Sato, T., *et al.* (1995) Helical polymer with a cooperative response to chiral information. *Science*, **268** (5219), 1860–1866.
[44] Ishi-i, T., Crego-Calama, M., Timmerman, P., *et al.* (2002) Enantioselective formation of a dynamic hydrogen-bonded assembly based on the chiral memory concept. *J. Am. Chem. Soc.*, **124** (49), 14631–14641.
[45] Green, M. M., Garetz, B. A., Munoz, B., *et al.* (1995) Majority rules in the copolymerization of mirror image isomers. *J. Am. Chem. Soc.*, **117** (14), 4181–4182.
[46] van Gestel, J., Palmans, A. R. A., Titulaer, B., *et al.* (2005) "Majority-rules" operative in chiral columnar stacks of C_3-symmetrical molecules. *J. Am. Chem. Soc.*, **127** (15), 5490–5494.
[47] Huang, X., Rickman, B. H., Borhan, B., *et al.* (1998) Zinc porphyrin tweezer in host-guest complexation: Determination of absolute configurations of diamines, amino acids, and amino alcohols by circular dichroism. *J. Am. Chem. Soc.*, **120** (24), 6185–6186.
[48] Bentley, K. W., Wolf, C. (2013) Stereodynamic chemosensor with selective circular dichroism and fluorescence readout for in situ determination of absolute configuration, enantiomeric excesses, and concentration of chiral compounds. *J. Am. Chem. Soc.*, **135** (33), 12200–12203.
[49] Girard, C., Kagan, H. B. (1998) Nonlinear effects in asymmetric catalysis and stereoselective reactions: ten years of investigation. *Angew. Chem. Int. Ed.*, **37** (21), 2922–2959.
[50] Haberhauer, G., Kallweit, C. (2010) A bridged azobenzene derivative as a reversible, light-induced chirality switch. *Angew. Chem. Int. Ed.*, **49** (13), 2418–2421.
[51] Johnson, R. S., Yamazaki, T., Kovalenko, A., Fenneri, H. (2007) Molecular basis for water-promoted supramolecular chirality inversion in helical rosette nanotubes. *J. Am. Chem. Soc.*, **129** (17), 5735–5743.
[52] Eelkema, R., Feringa, B. L. (2006) Phosphoric acids as amplifiers of molecular chirality in liquid crystalline media. *Org. Lett.*, **8** (7), 1331–1334.
[53] Haino, T., Tanaka, T., Fukazawa, Y. (2008) Self-assembly of tris(phenylisoxazolyl)benzene and its asymmetric induction of supramolecular chirality. *Chem. Commun.,* 468–470.
[54] Forgan, R. S., Sauvage, J.-P., Stoddart, J. F. (2011) Chemical topology: complex molecular knots, links, and entanglements. *Chem. Rev.*, **111** (9), 5434–5464.
[55] Simon, J. (1986) Topological chirality of certain molecules. *Topology*, **25** (2), 229–235.
[56] Flapan, E. (1991) Topological techniques to detect chirality. In *New Developments in Molecular Chirality*, (ed. P. G. Mezey), pp. 209–239. Kluwer Academic Publishers.

[57] Chambron, J.-C., Sauvage, J.-P., Mislow, K., *et al.* (2001) A [2]catenane and a [2]rotaxane as prototypes of topological and Euclidean molecular "rubber gloves." *Chem. Eur. J.*, **7** (19), 4085–4096.
[58] McArdle, C. P., Jennings, M. C., Vittal, J. J., Puddephatt, R. J. (2001) Self-assembly of rings, catenanes, and a doubly braided catenane containing gold(I): the hinge-group effect in diacetylide ligands. *Chem. Eur. J.*, **7** (16), 3572–3583.
[59] Ponnuswamy, N., Cougnon, F. B. L., Clough, J. M., *et al.* (2012) Discovery of an organic trefoil knot. *Science*, **338** (6108), 783–785.
[60] Pentecost, C. D., Chichak, K. S., Peters, A., *et al.* (2007) A molecular Solomon link. *Angew. Chem. Int. Ed.*, **46** (1–2), 218–222.
[61] Peinador, C., Blanco, V., Quíntela, J. M. (2009) A new doubly interlocked [2]catenane. *J. Am. Chem. Soc.*, **131** (3), 920–921.
[62] Ponnuswamy, N., Cougnon, F. B. L., Dan Pantoş, G. Sanders, J. K. M. (2014) Homochiral and *meso* figure eight knots and a Solomon link. *J. Am. Chem. Soc.*, **136** (23), 8243–8251.
[63] Mitchell, D. K., Sauvage, J.-P. (1988) A topologically chiral [2]catenand. *Angew. Chem. Int. Ed. Engl.*, **27** (7), 930–931.
[64] Chambron, J.-C., Mitchell, D. K., Sauvage, J.-P. (1992) Synthesis, characterization, and a proton NMR study of topologically chiral copper(I) [2]-catenates and achiral analogues. *J. Am. Chem. Soc.*, **114** (12), 4625–4631.
[65] Kaida, Y., Okamoto, Y., Chambron, *et al.* (1993) The separation of optically-active copper(I) catenates. *Tetrahedron Lett.*, **34** (6), 1019–1022.
[66] Jäger, R., Vögtle, F. (1997) A new synthetic strategy towards molecules with mechanical bonds: Nonionic template synthesis of amide-linked catenanes and rotaxanes. *Angew. Chem. Int. Ed.*, **36** (9), 930–944.
[67] Ottens-Hildebrandt, S., Schmidt, T., Harren, J., Vögtle, F. (1995) Sulfonamide-based catenanes – Regioselective template synthesis. *Liebigs Ann.* (10), 1855–1860.
[68] Yamamoto, C., Okamoto, Y., Schmidt, T., *et al.* (1997) Enantiomeric resolution of cycloenantiomeric rotaxane, topologically chiral catenane, and pretzel-shaped molecules: Observation of pronounced circular dichroism. *J. Am. Chem. Soc.*, **119** (43), 10547–10548.
[69] Nierengarten, J.-F., Dietrich-Buchecker, C. O., Sauvage, J.-P. (1994) Synthesis of a doubly interlocked [2]-catenane. *J. Am. Chem. Soc.*, **116** (1), 375–376.
[70] Dietrich-Buchecker, C., Sauvage, J.-P. (1999) Lithium templated synthesis of catenanes: Efficient synthesis of doubly interlocked [2]-catenanes. *Chem. Commun.*, 615–616.
[71] Chambron, J.-C., Sauvage, J.-P. (2013) Topologically complex molecules obtained by transition metal templation: It is the presentation that determines the synthesis strategy. *New J. Chem.*, **37**, 49–57.
[72] Dietrich-Buchecker, C. O., Nierengarten, J.-F., Sauvage, J.-P., *et al.* (1993) Dicopper(I) trefoil knots and related unknotted molecular systems: Influence of ring size and structural factors on their synthesis and electrochemical and excited state properties. *J. Am. Chem. Soc.*, **115** (24), 11237–11244.
[73] Dietrich-Buchecker, C. O., Sauvage, J.-P., Kintzinger, J.-P., *et al.* (1992) A di-copper(I) trefoil knot and its parent ring compounds: Synthesis, solution studies and X-ray structures. *New J. Chem.*, **16**, 931–942.
[74] Rapenne, G., Dietrich-Buchecker, C., Sauvage, J.-P. (1999) Copper(I)- or iron(II)- templated synthesis of molecular knots containing two tetrahedral or octahedral coordination sites. *J. Am. Chem. Soc.*, **121** (5), 994–1001.
[75] Perret-Aebi, L.-E., von Zelewsky, A., Dietrich-Buchecker, C., Sauvage, J.-P. (2004) Stereoselective synthesis of a topologically chiral molecule: The trefoil knot. *Angew. Chem. Int. Ed.*, **43** (34), 4482–4485.
[76] Cao, P.-F., Mangadlao, J., Advincula, R. (2015) A trefoil knotted polymer produced through ring expansion. *Angew. Chem. Int. Ed.*, **54** (17), 5127–5131.
[77] Safarowski, O., Nieger, M., Fröhlich, R., Vögtle, F. (2000) A molecular knot with twelve amide groups–One-step synthesis, crystal structure, chirality. *Angew. Chem. Int. Ed.*, **39** (9), 1616–1618.

[78] Vögtle, F., Hünten, A., Vogel, E., *et al.* (2001) Novel amide-based molecular knots: Complete enantiomeric separation, chiroptical properties, and absolute configuration. *Angew. Chem. Int. Ed.*, **40** (13), 2468–2471.
[79] Feigel, M., Ladberg, R., Engels, S., *et al.* (2006) A trefoil knot made of amino-acids and steroids. *Angew. Chem. Int. Ed.*, **45** (34), 5698–5702.
[80] Hasenknopf, B., Lehn, J.-M., Boumediene, N., *et al.* (1997) Self-assembly of tetra- and hexanuclear circular helicates. *J. Am. Chem. Soc.*, **119** (45), 10956–10962.
[81] Ayme, J.-F., Beves, J. E., Leigh, D. A., *et al.* (2012) A synthetic molecular pentafoil knot. *Nat. Chem.*, **4** (1), 15–20.